

Review of aeronautical fatigue and structural integrity investigations in the Netherlands during the period March 2019 - March 2021

Review of aeronautical fatigue and structural integrity investigations in the Netherlands during the period March 2019 - March 2021

R.C. Alderliesten

Abstract

This report is a review of the aeronautical fatigue and structural integrity activities in the Netherlands during the period March 2019 to March 2021. The review is the Netherlands National Delegate's contribution to the International Committee on Aeronautical Fatigue and Structural Integrity (ICAF) published on the ICAF website in June 2021.

An electronic version of this review is available at <https://www.icafe.aero/>.

Table of Contents

Abbreviations	5
1. Introduction	6
2. Metal Fatigue.....	7
2.1. Interaction between stress ranges and stress ratios during variable amplitude fatigue loading.....	7
2.2. Prediction of fatigue in engineering alloys (PROF)	8
2.3. On the plastic dissipation during fatigue crack growth.....	10
2.4. The fatigue performance of various aluminum alloys pretreated with Cr(VI)-free anodizing processes for both bonding and non-bonding applications.....	11
2.5. Additive Manufacturing and Certification of Flight Critical part	14
2.6. Short/small fatigue crack growth, thresholds and environmental effects: a tale of two engineering paradigms.....	16
3. Composites & Fibre Metal Laminates	18
3.1. Determination of Mode I Fatigue Delamination Propagation in Unidirectional Fibre-Reinforced Polymer Composites.....	18
3.2. Constant Life Diagrams for Composites	18
3.3. Fatigue analysis of composite materials using a continuum damage mechanics framework	19
3.4. Fatigue testing on Glare FML panel containing transition to full-GFRP composite (ACASIAS project WP5 “Smart FML Panel”).....	22
3.5. Residual strength of impact damage in skin and skin-stringer interface in thermoplastic orthogrid fuselage panels.....	26
3.6. Characterization of delamination onset and propagation under fatigue loading of AS4D/PEKK-FC thermoplastic composites.....	28
3.7. Unfolding the Early Fatigue Damage Process for CFRP Cross-Ply Laminates	30
4. Prognostics & Risk Analysis	33
4.1. Adaptive Prognostics for Remaining Useful life of Composite Structures	33
4.2. Probabilistic Fail-Safe structural risk analyses.....	35
4.3. Predicting helicopter damage caused by a collision with an Unmanned Aerial System using explicit Finite Element Analysis	36
5. Non-Destructive Evaluation.....	39
5.1. Load monitoring of cantilever structures using a single optical fibre.....	39
5.2. Automatic fusion of different Non-Destructive Inspection techniques.....	41
6. Structural Health & Usage Monitoring.....	43
6.1. Landing gear health monitoring	43
6.2. Multiple load path damage detection with optical fibre Bragg grating sensors	45
6.3. Structural Health Monitoring of Composite Structures by Fusing Sensor Data	46

7.	Fleet Life Management	49
7.1.	Individual tracking of RNLAf aircraft.....	49
8.	Special Category.....	50
8.1.	Impact of additive manufacturing on structural integrity methodologies.....	50
8.2.	Quantitative Fractography Applications for Fatigue Fracture Surfaces	50
8.3.	Milestone case histories in aircraft structural integrity	51
8.4.	Short/small fatigue crack growth, thresholds and environmental effects.....	52
	References.....	53

Abbreviations

AE	Acoustic Emission
AM	Additive Manufacturing
CA	Constant Amplitude
CFRP	Carbon fibre reinforced polymer composites
CLD	Constant Life Diagram
DCB	Double Cantilever Beam
DIC	Digital Image Correlation
FBG	Fibre-Bragg Grating
FCG	Fatigue Crack Growth
FEA	Finite Element Analysis
FML	Fibre Metal Laminate
GFRP	Glass fibre reinforced polymer composites
HIP	High Isostatic Pressure
LEFM	Linear Elastic Fracture Mechanics
PROF	PRediction Of Fatigue in engineering alloys
QF	Quantitative Fractography
RNLAF	Royal Netherlands Air Force
RUL	Remaining Useful Life
SHM	Structural Health Monitoring
SRA	Structural Risk Analysis
UD	Unidirectional
VA	Variable Amplitude

1. Introduction

The present report provides an overview of the work and research performed in the Netherlands in the field of aeronautical fatigue and structural integrity during the period from March 2019 until March 2021. The subjects in this review come from the following contributors:

- Delft University of Technology (TU Delft)
- GKN Aerospace-Fokker (GKN Fokker)
- Royal Netherlands Aerospace Centre (NLR)
- Royal Netherlands Air Force (RNLAf)
- Ministry of Defence (MoD)

Additionally, collaborative work between the NLR and the Defence Science and technology Group (DST-G) of Australia, and between TU Delft and various European universities and institutes is included.

The names of the principal investigators and their affiliations are provided at the start of each subject. The format and arrangement of this review is similar to that of previous national reviews.

2. Metal Fatigue

2.1. Interaction between stress ranges and stress ratios during variable amplitude fatigue loading

Jesse van Kuijk, René Alderliesten (TU Delft)

This PhD research project focuses on the physics underlying constant and variable amplitude (VA) fatigue crack growth in relation to stress ranges and opening/closing stresses [1]. The concepts of physics considered are the application of strain energy (work) when loading, and the dissipation of energy through plasticity and the formation crack surfaces.

Fatigue tests on aluminium 2024-T3 CCT specimens with through-cracks were performed to study the crack growth, accurately measured with the potential drop technique (PDT). This PDT was improved to perform measurements through the fatigue load cycle, effectively measuring the effect of crack tip plasticity [2]. The electrical resistivity changes with deformation, where the Poisson's effect and piezo-resistivity work against each other. While the resultant signal initially changes proportional to the applied loading cycle, a clear plateau is formed at the moment the crack opens. This plateau ends when the crack closes where the signal decays proportionally to the load cycle again, see Figure 1. Through these direct-measurements the moment crack opening and closure and the magnitude of corresponding stresses can be established. This correlation was verified through high-speed DIC measurement at the crack tip, with which the growth, translation and shrinkage of the plastic zone could be observed throughout the load cycle.

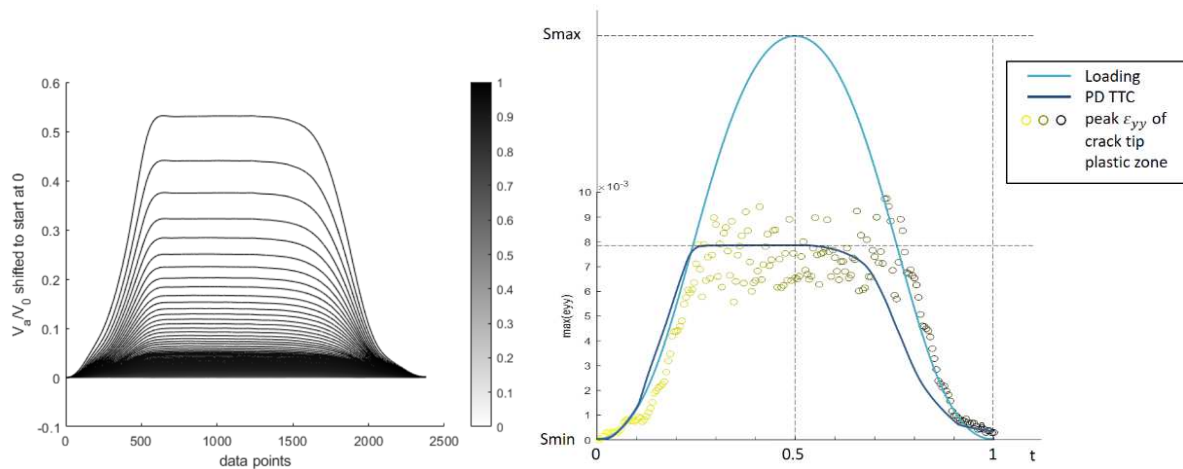


Figure 1 PDT signal variation through the loading cycles (curves have been translated – not scaled – to start at $V_a/V_0 = 0$) (left), comparison between the measured peak strain ϵ_{yy} , the PDT signal and a schematic of the stress cycle (right) [3]

Through using concepts from physics, an energy balance for crack growth was developed, assessing the elastic, plastic, and crack growth energy (dissipation) components of a cracked plate undergoing constant amplitude fatigue loading. To understand how these components change with increasing crack length and time, a theoretical model is developed that explicitly describes the various energy components during crack growth. A key insight from this energy balance is that in the physics-description the balance is continuous, and the number of cycles N does not constitute a variable. This is interpreted as that the energy balance characterises the effective resistance to growth, which is

descriptive and through relating to applied loading (work or strain energy) may provide a predictive model. A first concept of prediction is proposed with recommendation to further develop this in a follow-up research project.

2.2. Prediction of fatigue in engineering alloys (PROF)

Emiel Amsterdam (NLR)

In 2016 Royal NLR started a four year project with Fokker, Embraer, Airbus, Lloyd's Register and Wärtsilä. The Delft University of Technology and the Royal Netherlands Air Force were also involved in the project. The objective of the project "Prediction of fatigue in engineering alloys (PROF)" is to improve the physical understanding and prediction of fatigue in engineering alloys. In the project it is clearly demonstrated that crack growth in AA 7075-T7351 shows a power law relationship with ΔK at all tested length scales/ ΔK values. The power law behaviour at all crack lengths, the introduction of the pivot points and modern computer technology allow fitting of the a-N curve to obtain crack growth rates without any noise (see Figure 2 and Figure 3). This replaces the method of incremental polynomial fitting, which introduces noise and errors in the crack growth rate results (see Figure 3). The ability to obtain very accurate crack growth rates will require less testing in the future and opens up a whole range of opportunities for understanding crack growth in ductile materials. It has been used, for example, to exactly determine the influence of small factors such as temperature, humidity and frequency. The new fitting method was presented to the ASTM E647 fatigue crack growth testing committee in Denver, 2019 [4].

The fitting method was also used to determine the effect of stress ratio and maximum stress on the fatigue crack growth rate (FCGR). This eventually led to the definition of a new, physics based, parameter of similitude and a new fatigue crack growth rate equation. Fatigue crack growth during variable amplitude (VA) testing also exhibits power law behavior between pivot points [5] and the new crack growth equation is able to correlate constant amplitude FCGR to variable amplitude FCGR. This knowledge was disseminated amongst the partners and will be published soon. It has also been used to make a blind prediction for DST Group's ASSIST challenge on military transport long cracks (ASSIST was formerly known as TITANS). NLR's blind prediction was closed to the experimental results [6].

The project ended in December 2019. A second PROF project will start in 2021 and is open to participants until 2022.

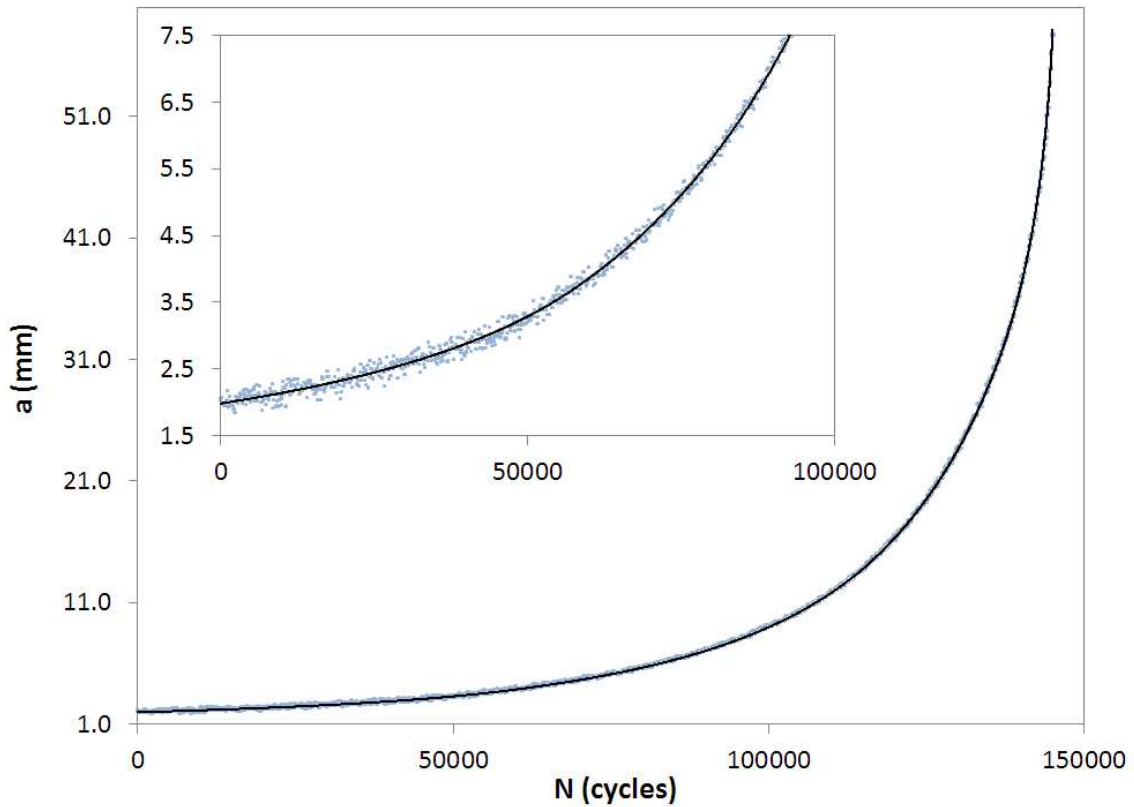


Figure 2 Crack length vs. cycles (a - N) curve for an arbitrary AA 7075-T7351 middle tension specimen. The crack lengths (blue dots) are measured with DCPD and the black line represents the best fit. The insert shows the same data for smaller crack lengths only

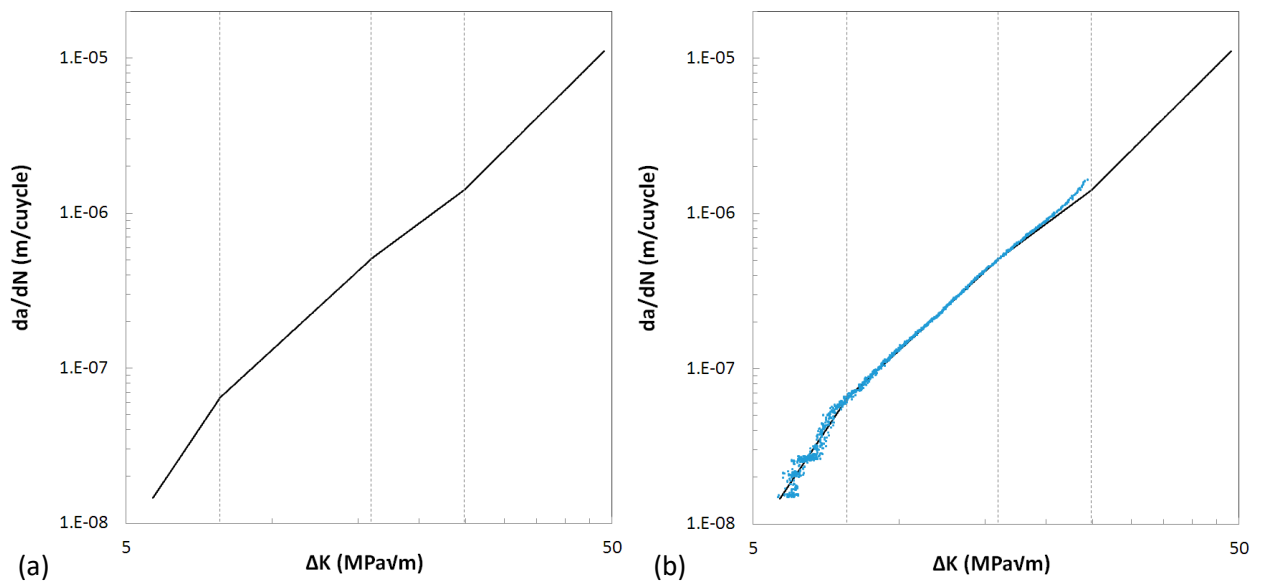


Figure 3 (a) Crack growth rate obtained by fitting the entire a - N curve using pivot points. The dashed lines indicate the pivot points, (b) Crack growth rates obtained by incremental polynomial fitting of the DCPD crack lengths using 401 data points

2.3. On the plastic dissipation during fatigue crack growth

Hongwei Quan, René Alderliesten (TU Delft)

Although Linear Elastic Fracture Mechanics (LEFM) has been applied successfully to practical engineering fatigue problems through the use of the Paris relation, it does not take into account explicitly the plasticity phenomena that strongly influence fatigue crack growth rates (da/dN). In this study, the fatigue crack phenomena were studied from a physical perspective. An energy approach was chosen because its universality for various materials, and because plasticity itself represents an important type of energy dissipation for metallic materials.

Currently, literature [7,8] correlates either the total plastic dissipation per cycle (dW_{tot}/dN) or the plastic dissipation in the reversed plastic zone per cycle (dW_{re}/dN) with fatigue crack growth rate (da/dN), and a linear relation is proposed. In order to prove or disprove such relationship, experiments on 7075-T6 central crack tension fatigue crack growth test were performed.

During the test the fatigue crack length was measured by visual method. The displacement fields around crack were measured with Digital Image Correlation (DIC). Then the measured displacement fields were applied as boundary conditions in Finite Element Analysis (FEA) of the experimental specimen to obtain the values of dW_{tot}/dN and dW_{re}/dN .

From the results, it is concluded that for 7075-T6 the linear relation between either dW_{tot}/dN or dW_{re}/dN and da/dN is incorrect. Both dW_{tot}/dN and dW_{re}/dN can be fitted with a power law to ΔK with an exponent of about 4, while the exponent in the Paris relation was 2.2 at $R=0.1$. The values of dW_{tot}/da and dW_{re}/da at $R=0.1$ increase instead rather than stay constant with da/dN as illustrated in Figure 4.

This implies that the plastic dissipation in a cycle, dU_{pl}/dN , is not an effective similitude parameter. From a physical perspective, the energy balance for fatigue crack growth can be described as

$$\frac{dW}{dN} = \frac{dU_a}{dN} + \frac{dU_{pl}}{dN} + \frac{dU_e}{dN}$$

The physical meaning of this equation is that the total dissipated energy during one cycle dW/dN is the sum of the energy dissipation for the new fatigue crack surface formation dU_a/dN , the plastic dissipation during one cycle dU_{pl}/dN and the elastic strain energy change after one cycle dU_e/dN . The fatigue crack propagation is only directly related to dU_a/dN , while dU_{pl}/dN and dU_e/dN are merely consequences of the fatigue crack growth.

Theoretically, the crack surface forming energy is the proper similitude parameter that can be directly linked to fatigue crack growth, instead of the plastic energy dissipation. However, the value of dU_a/dN is too small to be measured accurately in reality. Therefore, the dU_{pl}/dN seems to be the only option left for that its value can be obtained. However, based on the current study one should be aware that plastic dissipation and fatigue crack growth are not straightforwardly related, and some extra efforts are needed to link these quantities.

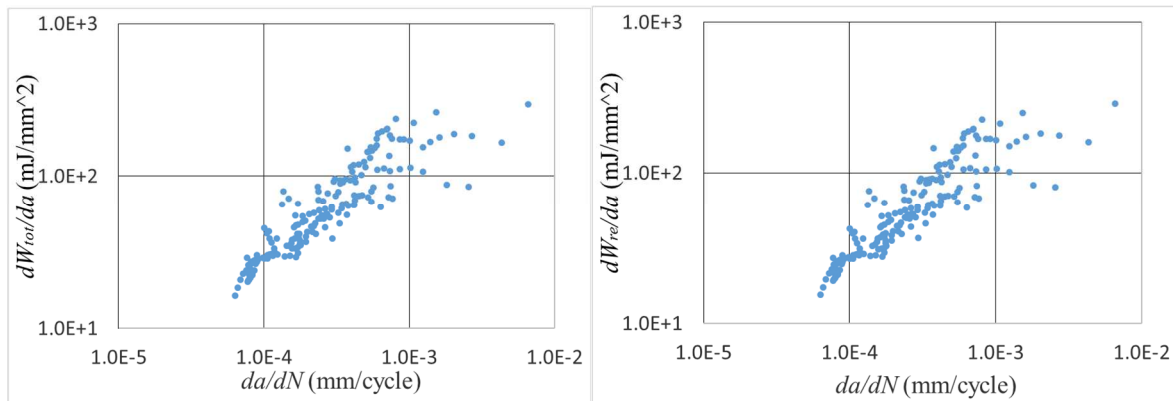


Figure 4 Total plastic dissipation per unit fatigue crack growth against da/dN (left), and plastic dissipation in the reversed plastic zone per unit fatigue crack growth against da/dN (right)

2.4. The fatigue performance of various aluminum alloys pretreated with Cr(VI)-free anodizing processes for both bonding and non-bonding applications

T. Janssen, J.M.M. de Kok, J.C.J. Hofstede (GKN Fokker)

To comply with the European REACH legislation, GKN Fokker will move from using Chromic Acid Anodizing (CAA) as surface treatment for corrosion protection purposes for bonding applications as well as for non-bonding applications to a number of REACH compliant chemical surface treatment processes. For bonding applications, this process is Phosphoric Sulfuric Acid Anodizing (PSA), while processes Thin Film Sulfuric Acid Anodizing (TFSA), Phosphoric Sulfuric Acid Anodizing (PSA) and Tartaric Sulfuric Acid Anodizing (TSA) will be used for non-bonding applications. GKN Fokker develops and maintains its own material- and process specifications, in combination with which the company's own Strength Handbook provides applicable strength data.

New, Cr(VI)-free processes were developed and qualified within the Materials & Processes department. In order to avoid part-specific certification efforts, the aim of the process qualification was to demonstrate a robust process that has at least equal performance as the CAA process. In this way, a gradual transition to the new treatment processes could be made, without the need for expensive drawing changes.

As part of the qualification of these processes, the results of an extensive fatigue testing campaign, performed with relevant aluminum alloys, were evaluated to assess the effect of the combinations of pre-penetrant etching and post-penetrant anodizing on the fatigue properties. About 900 notched fatigue specimens with a relatively low stress concentration ($K_t = 1.35 - 1.4$) and standard manufacturing quality and surface roughness were subjected to cyclic tension-tension loading ($R = 0.1$) in LT-grain direction. For 7050-T7451 thick plate alloy, known to be sensitive to chromic acid pickling treatments, also tests were performed for $R = -1$ and in ST-grain direction.

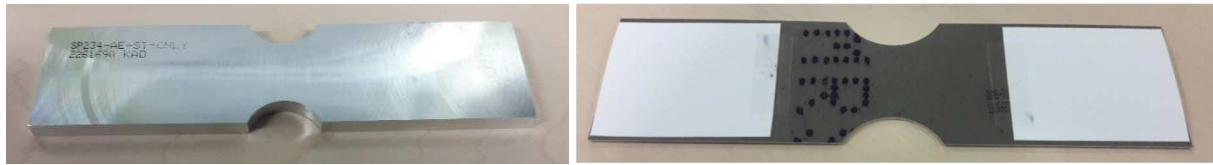


Figure 5 Typical examples of low K_t dogbone fatigue specimens

Specimens from plate alloys were extracted from the centre of the billet to represent worst case grain structure, highest sensitivity to pickling and anodizing treatment and therefore worst case fatigue properties. Specimens from (both bare and clad) sheet alloys were all machined from 1 mm stock material.

Bonding applications

For sheet metal bonding applications, several variations of the PSA anodizing process have been tested. Process parameters (typically temperature and voltage) were selected to represent the baseline PSA process and to obtain a wide range of anodic oxide layer thicknesses. The anodic layer thickness variation has been verified by thickness measurements (SEM) and coating weight on samples from fatigue specimens. The presence of intergranular attack / end grain pitting (IGA / EGP) was verified on various samples as well.

A strong correlation between the intended process variations, anodic coating weight and layer thickness was observed for 2024 and 7075 alloys, both in bare and clad materials, while on most specimens no significant IGA/EGP was observed. For bare sheet materials, developing a significantly lower anodic coating weight than the clad materials, the number of fatigue cycles to fracture did not change with increasing coating weight within the tested variation. For clad sheet however, the anodic coating weight was larger and a more significant effect on the number of cycles to fracture was observed, leading to the definition of clear process window boundaries. With this test campaign, it could be shown that the Fokker PSA process has coating weights below the maximum values for acceptable fatigue performance.

Non-bonding applications

For non-bonding applications, similar IGA/EGP measurements were taken from the specimens, which were not only treated with an anodizing step, but also with several pickling and desmutting steps that are needed before a penetrant inspection step normally required for machined components.

Anodic coating weights due to the anodizing process step were in the range of expected values based on the results from the sheet materials.

Fatigue tests were typically performed in the range of $10^3 - 10^7$ cycles. All plate alloys showed a clear transition from the 'Basquin-domain' towards a fatigue limit, regardless of the applied treatments. Test results were used for various curve-fitting procedures, including a power-law fit for the Basquin-domain, the staircase method for determination of the fatigue limit and a four-parameter Weibull equation covering the entire range of fatigue cycles to fracture. For each alloy-treatment combination, results from these the fitting processes are highly comparable and were useful for the comparative evaluation between the various processes. In addition, a statistical comparison between the data sets was performed, which assisted the evaluation when comparison of the fitted curves was inconclusive.

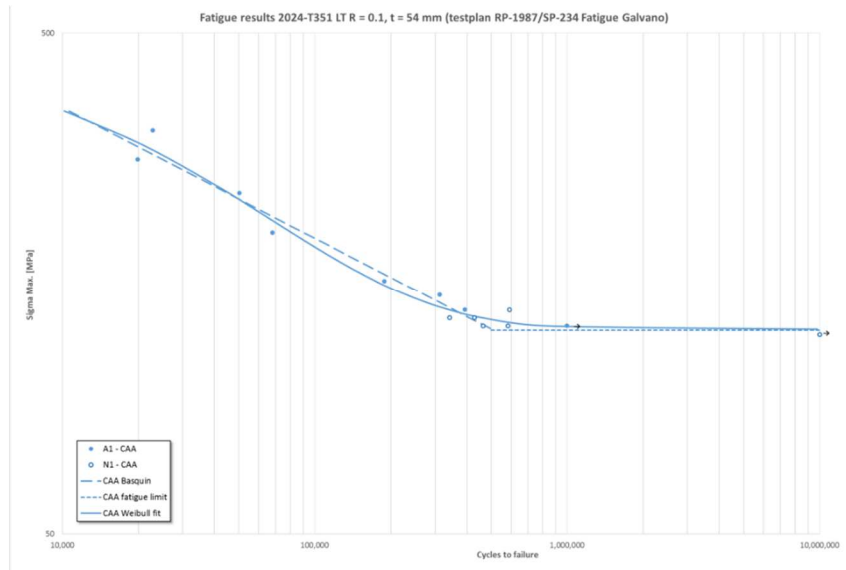


Figure 6 Typical shape of fatigue life curve

The results for TFSAA, PSA and TSA are evaluated and compared with the results obtained for the standard CAA process for each of the aluminium alloys tested, which showed that:

- PSA, TFSAA and TSA have shown acceptable fatigue strength compared to CAA for sheet alloys AA2024-T3 clad, AA7075-T6 clad, AA7075-T6 bare and for plate alloys AA2024-T351 and AA7075-T7351.
- PSA has shown acceptable fatigue strength also for sheet alloy AA2024-T3 bare.
- TFSAA has shown acceptable fatigue strength also for plate alloy AA7050-T7451.

Based on the fatigue test results, the various anodizing processes (the last treatment step in the chain) were demonstrated to have no significantly different effect on the fatigue properties than the reference CAA process.

However, it was well known from literature (and confirmed during the test campaign) that the 7050-T7451 alloy would be sensitive to the severity of the chromic acid etching process normally applied to machined parts for crack inspections.

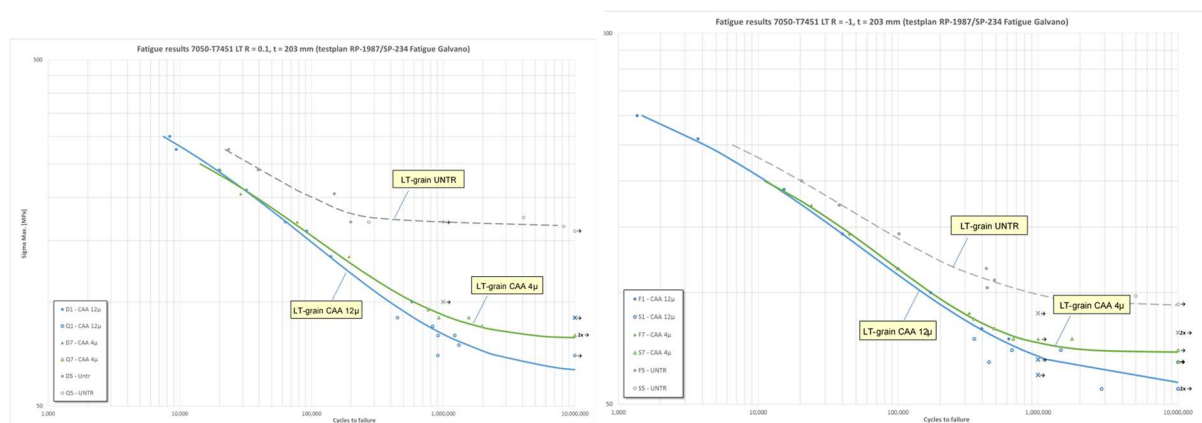


Figure 7 Effect of amount of metal removal (CAA) on especially the fatigue limit for 7050-T7451 alloy

Although the pre-penetrant treatment steps were Cr(VI) free and the sensitivity to the amount of metal removal was not expected, the various etching/pickling processes were shown to significantly affect the fatigue properties of some alloys as well, especially in the fatigue limit domain. Recommendations were made for the maximum allowed metal removal in order to limit the amount of end grain pitting to an acceptable level. It is expected that a second test campaign for the relevant alloys will confirm these recommendations in the near future.

2.5. Additive Manufacturing and Certification of Flight Critical part

H.N. Kamphuis, M. Bosman, T. Janssen (GKN Fokker), C.D. Rans (TU Delft), M. van Hintem (MoD), G.A. Kool, E. Amsterdam (NLR)

The aim of the project is to contribute to the acceptance of additive manufacturing (AM) technology by producing, certifying and flying a Flight Critical AM produced part. This raises the bar compared to non-flight critical parts, because of the more stringent regulations for Flight Critical parts. In this project the goal is to replace an existing conventional machined Flight Critical part by a geometrical identical AM produced and certified part. Part substitution is not where the AM process has the greatest added value (see Figure 8), however it is the next step in acceptance of the AM technology.

The selected Flight Critical part for substitution is a titanium component of a helicopter door hinge.

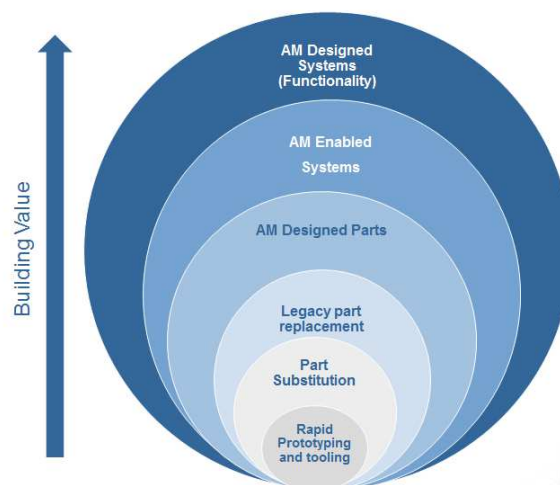


Figure 8 Value increase of AM process

The Flight Critical part will be created by the Laser Powder Bed Fusion (L-PBF) process, followed by heat treatment and machining operation. All surfaces will be machined, similarly to the substituted part, with the beneficial effect that the surface effects will be removed (particular the surface roughness improves). High Isostatic Pressure (HIP) treatment is a commonly applied process to reduce internal imperfections in AM produced parts. However, this is a costly process. The aim is to certify the part without using the HIP process.

Certification

The challenge of metal additive manufacturing lies in the fact that the bulk material is created while building the part and one cannot rely on standard material properties established by the raw material supplier. The material properties need to be proven consistent because they depend on the feed stock material, the process parameters and the shape of the part.

Certification supported by test evidence is required to demonstrate that the Flight Critical part is airworthy. Generally 2 certification approaches can be distinguished:

1. Part certification
2. Process certification

Part certification is currently the common used approach to certify AM parts, because AM process standards are in development. Part certification requires the least effort compared to process certification.

The Flight Critical AM part will be certified against full strength requirements. Besides the static loads, the part is loaded for fatigue, both in the high cycle fatigue range ($N = 10^4 - 10^6$) and in the very high cycle fatigue range ($N \approx 10^9$).

To demonstrate the strength requirements, test specimens have been produced with generally available Ti-6Al-4V powder and tested (see Figure 9). The manufacturing conditions of the specimens are equal to the substitute part (i.e. AM process parameters, heat treatment, machined surface, etc.).

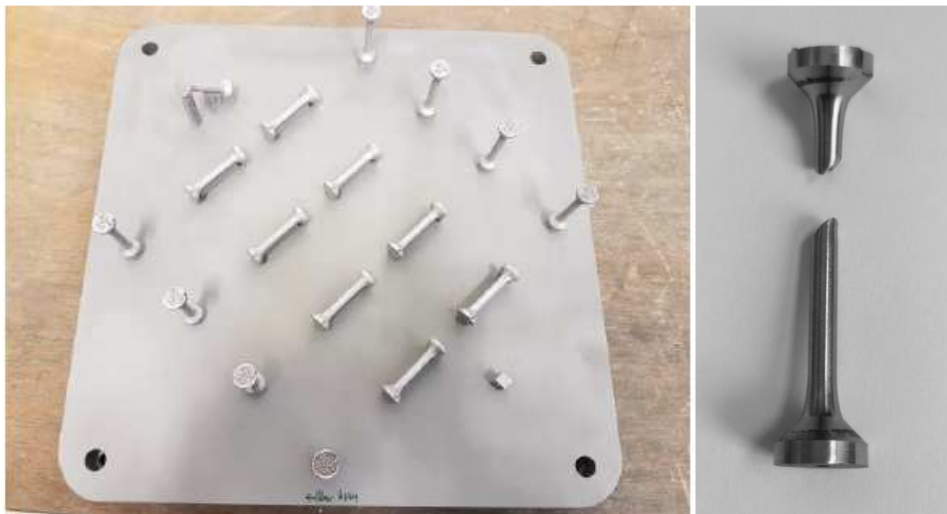


Figure 9 AM produced test specimens (left) and tested specimen (right)

The specimens are tested for both static and fatigue strength values. With the test results the mean S-N curve is generated to validate the high cycle fatigue properties (see Figure 10). These tests ran between $N = 10^4 - 10^6$ cycles. This curve is conservatively extrapolated to obtain the very high cycle fatigue properties at $N = 10^9$.

Relative large scatter in the fatigue properties is one of the challenges of the AM process. The test results confirm that the scatter is an order of magnitude (see Figure 10). Also the fact that the specimens have had no HIP treatment is not beneficial in reducing the scatter.

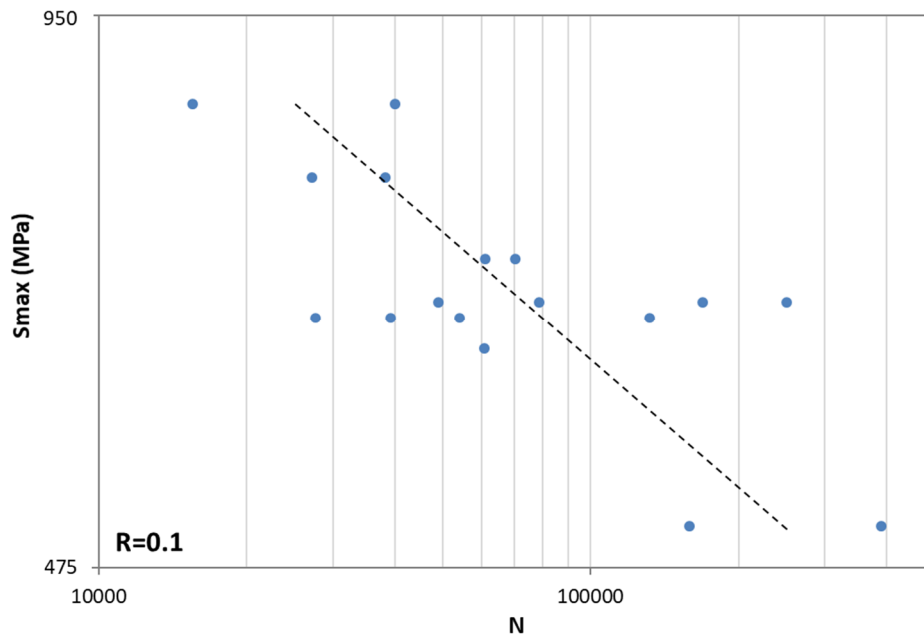


Figure 10 S-N curve for Ti-6Al-4V AM test specimens that failed by fatigue initiation at the surface

After completion of the specimen testing, the actual helicopter part is produced and tested by cut-up testing and microstructure investigation.

The specimen test results are promising and the possibility to certify the part was deemed realistic, also accounting for fact that the test results show a significant variation in mechanical properties. However, when evaluating the results in more detail, on some locations of the build, a strong dependency to location- or build-plate configuration dependency was observed. Therefore, given that material properties depend on the position in the building chamber or the presence of other parts in the same build, it could not be demonstrated with sufficient confidence that the part that was not cut-up would exhibit the same properties and strength values as the samples that were used for the determination of the strength properties. Understanding the root cause of the location- or build-plate configuration dependency and improvements of the AM process are required in order to enable certification of the part.

This project has targeted substituting a Flight Critical conventional machined part by a geometrical identical AM produced part. The layer-by-layer build approach introduces many risks for errors on a microscale resulting in variation in material properties, including fatigue. The potential to certify the part is clearly visible, but this requires a better understanding and improvement of the AM process, in order to reduce the scatter and improve the material properties.

2.6. Short/small fatigue crack growth, thresholds and environmental effects: a tale of two engineering paradigms

Russell J. H. Wanhill (NLR), Stefanie E. Stanzl-Tschegg (Austria)

The paper [9] is the result of discussions about the review ‘When do small fatigue cracks propagate and when are they arrested?’ in Corrosion Reviews, 2019; 37(5): 397-418. These discussions arose from the two engineering paradigms characterizing fatigue research for (i) an aerospace research and technology remit for metallic airframes, and (ii) a materials science research programme supporting a methodology for steam turbine low pressure (LP) blade operations. This paper is in the spirit of

August Thum (1881-1957), who collated, adapted and published much fatigue literature from different sources for the benefit of engineers and designers. The paper is of cross-discipline interest for investigators of metal fatigue with respect to design requirements, life predictions and assessments. In more detail, the paper considers the similarities and differences in the fatigue design methodologies for airframes and steam turbine LP blades. This includes short/small fatigue cracks, fatigue crack growth thresholds, high-cycle fatigue (HCF) and very-high-cycle fatigue (VHCF), and the relevance of environmental effects (corrosion and corrosion fatigue).

3. Composites & Fibre Metal Laminates

3.1. Determination of Mode I Fatigue Delamination Propagation in Unidirectional Fibre-Reinforced Polymer Composites

René Alderliesten (TU Delft), Andreas Brunner (empa)

Although that standardized test methods are available to characterise quasi-static mode-I delamination fracture toughness (ISO 15024) and the fatigue delamination onset (ASTM D 6115), fatigue delamination propagation has not been standardized yet. Despite several initiatives and round robin exercises, no consensus has been achieved on how to evaluate the fatigue growth, in particular when large scale fibre bridging occurs.

This fibre bridging is generally attributed to the unidirectional lay-up adopted in the Double Cantilever Beam (DCB) specimen, which artificially increases the delamination resistance. This in most cases results in unconservative data, because the amount of fibre-bridging in structural applications is generally limited or even absent. Hence, for design, a "conservative" value is desirable. Quantifying the effects of fibre-bridging on delamination propagation in unidirectional laminates would allow for estimating the intrinsic delamination resistance and corresponding scatter of this laminate, satisfying the safety factor requirements defined in design guidelines.

To this aim, a test procedure is in development within ESIS-TC4 describing an experimental procedure to quantify and exclude the contribution of large-scale fibre bridging in mode I fatigue fracture tests of unidirectionally fibre-reinforced plastic composites. This test procedure comprises performing multiple sequences per specimen, to enable the derivation of a zero-bridging delamination resistance curve via regression through and translation of all data. This test procedure is a modification and extension of a former ESIS-TC4 test procedure, but also incorporates an analysis based on a modified Hartman-Schijve equation for the determination of scatter in the fatigue fracture curves (essentially da/dN versus a " $\sqrt{\Delta G}$ " related quantity instead of the "conventional" Paris-equation correlating da/dN with ΔK or ΔG). To demonstrate the repeatability and reproducibility of the test procedure, a round robin exercise is currently executed with participants of the ESIS-TC4 committee, but also other parties are invited to participate.

3.2. Constant Life Diagrams for Composites

Agnes Broer, Dimitrios Zarouchas (TU Delft)

Constant life diagrams (CLD) can be used to predict the fatigue life of composites subjected to constant amplitude (CA) fatigue loading based on a limited number of experimental S-N curves. As performing fatigue tests to determine the fatigue life is often expensive and time-consuming, the application of such CLD models can provide great benefits by reducing the number of to-be-performed tests. Kawai et al. [10] proposed such a CLD, called the anisomorphic CLD, which is capable of fatigue life prediction of carbon fibre-reinforced polymer (CFRP) coupons in tension-tension (T-T), tension-compression (T-C), and compression-compression (C-C) CA loading. The basic (two-segment) anisomorphic model requires as input only experimental data from a single S-N curve to predict fatigue life, but is limited in its applicability and accuracy for different loading ranges and lay-ups. To assess these limitations, Kawai et al. [11,12] also proposed more elaborate anisomorphic models (three- and four-segment) with

wider applications and more accurate predictions. Yet, these models require additional fatigue life input data corresponding to two and three S-N curves, respectively.

One of the main disadvantages of the anisomorphic model is that (part of) the fatigue life data required as input must be obtained under the critical R-ratio χ , which is defined as the ratio between the ultimate compressive strength and the ultimate tensile strength. This is unpractical as the R-ratio χ is not one of the common R-ratios such as $R=0.1$, $R=-1$, or $R=10$. This often means that, even if fatigue life data is already available, it cannot be used as input as the data has not been obtained under the appropriate critical R-ratio χ . Consequently, in order to implement the anisomorphic models from Kawai et al., users often need to perform additional fatigue life tests or make great assumptions that affect the accuracy of the fatigue life predictions.

In our work, we proposed an adapted anisomorphic model for CFRP composites that builds upon the model of Kawai et al. [10,11,12]. Yet its implementation is more practical as the input R-ratio has been adapted to one of the standard R-ratios: the proposed adapted anisomorphic model uses as input only fatigue life data obtained under either $R=0.1$ or $R=-1.0$ (an example of such an established CLD is shown in Figure 11). Moreover, only fatigue life data under a single S-N curve is required as input, based on which the adapted anisomorphic model is capable of predicting the fatigue life for T-T, T-C, and C-C CA loading for a variety of composite lay-ups. In this manner, the benefit of using only a single R-ratio as input is maintained and extended to more accurate fatigue life predictions for T-C and C-C loading of various lay-ups, while simultaneously the implementation of the CLD becomes more user-friendly and practical. The proposed adapted anisomorphic model was validated by collecting new fatigue life data during an experimental campaign.

Details of this work, including the fatigue life datasets, can be found in [13] and [14].

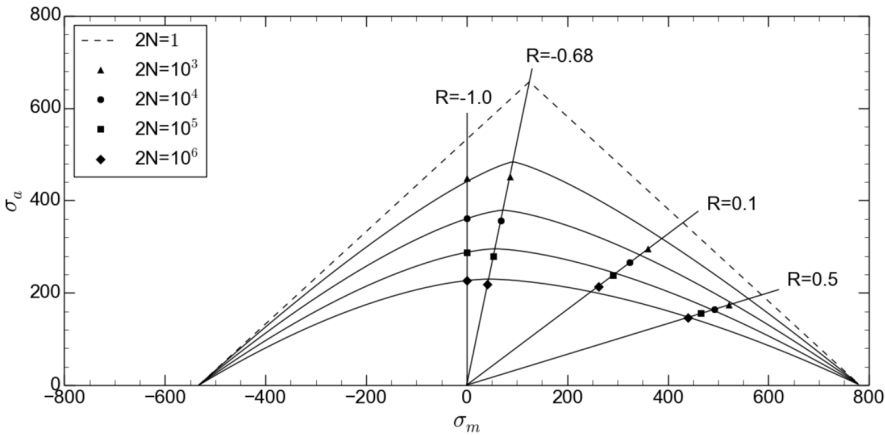


Figure 11 Example of a constant fatigue life diagram obtained using the adapted anisomorphic model and by using a single S-N curve ($R=-1.0$) as input, reprinted from [14].

3.3. Fatigue analysis of composite materials using a continuum damage mechanics framework

Jaykarna Bhangale, René Alderliesten (TU Delft)

To design the next generation wind turbine rotor blades, engineers need to improve blade fatigue life prediction for various materials used in the construction of blades. The challenge is to predict life expectancy and extent of damage after a specific load history. The research proposed is divided into

three sections to address this challenge. First, developing fundamental constitutive theory followed by mathematical formulation supporting the theory and finally, validating the theory and mathematical model to blade laminate and subcomponent level materials.

Thermodynamic theory for the irreversible process provides a generic theory valid for the entire fatigue phenomenon, as shown in Figure 12.

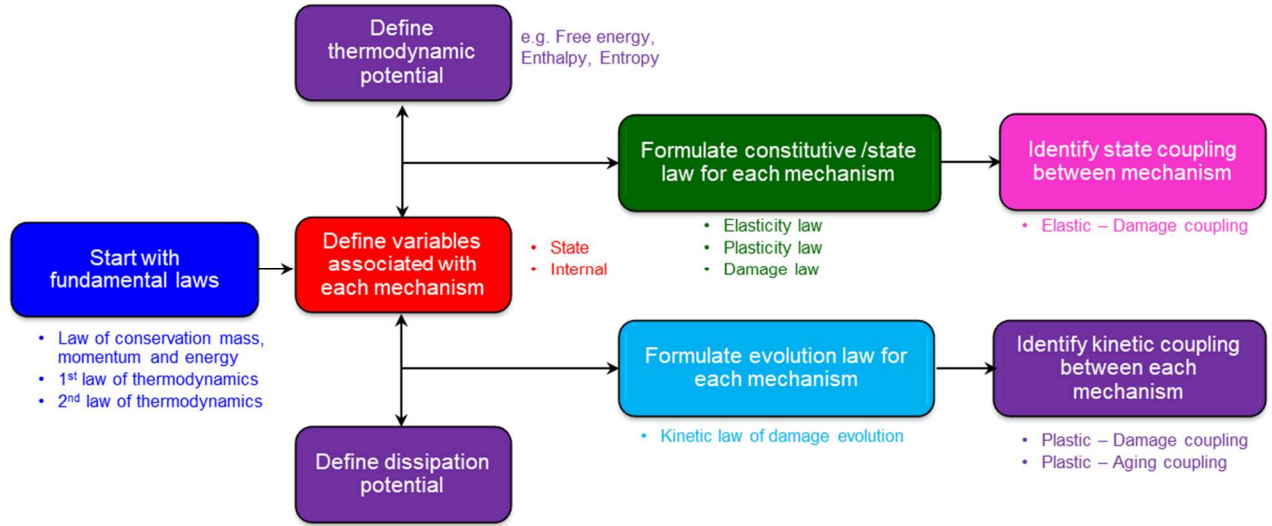


Figure 12 Thermodynamic theory for the irreversible process

The thermodynamic potential can be expressed as

$$\rho\psi = \frac{1}{2}E_{ijkl}\varepsilon_{ij}^e\varepsilon_{kl}^e(1-D) + R_\infty \left[r + \frac{1}{b} \exp(br) \right] + \frac{X_\infty}{3} \sum_i C_i \alpha_j \alpha_j + a(cr - L) + L - baT \text{tr}(\varepsilon^e) - \rho \frac{\bar{c}}{2T_0} T^2 + \dots \quad (1)$$

The blue part represents elastic potential, the parts with different shades of aqua colour represent inelastic (isotropic hardening, kinematic hardening and ageing) potential and the red part is thermal (linear thermo-elasticity and thermal expansion) contribution in the total potential of the material.

An analytical expression for the dissipation potential φ is

$$\varphi^* = (\sigma_{ij}^D - X_j^D)_{eq} - R - \sigma_y + \left[c - \beta \exp\left(-\gamma \frac{r}{1-D}\right) \right] + \frac{3}{4X_\infty} X_j^D X_j^D + [a_\infty - a]Z + \varphi_D^* + \frac{1k}{2T} \vec{g} \cdot \vec{g} + \dots \quad (2)$$

Here the orange part φ_D^* is the damage potential, while the other coloured components relate to the colours in Equation (1).

Using Lemaitre's [15] generalized representation for damage potential and the phenomenological relationship between inelastic strain and stress range, the final fatigue life N_F can be computed with

$$N_F = \left[\frac{KM(1-\alpha)}{2(M+1)\Delta\sigma^M} \right]^{\frac{1}{1-\alpha}} \quad (3)$$

Where K, M and α are model parameters. The damage state at any given cycle can be computed with

$$D = 1 - \left[1 - \left(\frac{N}{N_F} \right)^{1-\alpha} \right]^{\frac{1}{M+1}} \quad (4)$$

This constant life curve expression, equation (3), and non-linear damage accumulation law, equation (4) enable the characterization of the fatigue damage coupled with elastic and plastic deformation.

Various experimental programs were conducted using materials from wind turbine blade laminate and subcomponent scale for validation of both these models. Detailed observations were made during the experiments to correlate the fundamental constitutive theories underlying the different mechanisms of the fatigue phenomenon. The model validation is shown here only for one out of eight material configurations investigated. The constant life diagram (CLD) and the evolution of damage at various stress ratios are shown in Figure 13 and Figure 14.

One peculiar feature of (3) is that these constant lifelines do not meet at one point on the abscissa, as shown in Figure 13, representing the effect of creep at high mean stresses. The non-linear development of damage resembles closely with the generic damage development stages reported in the literature [16] and as shown in Figure 14. This resemblance makes the mathematical formulation consistent with the presented theory.

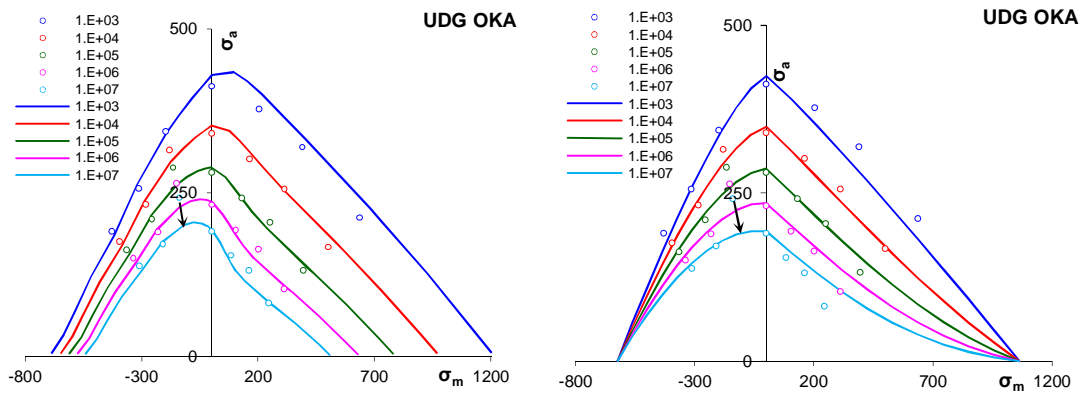


Figure 13 Constant Life Diagram for all UD material configurations; (left) using the CDM framework MAPE=131%, (right) using Multislope CLD model from the traditional framework MAPE=243%

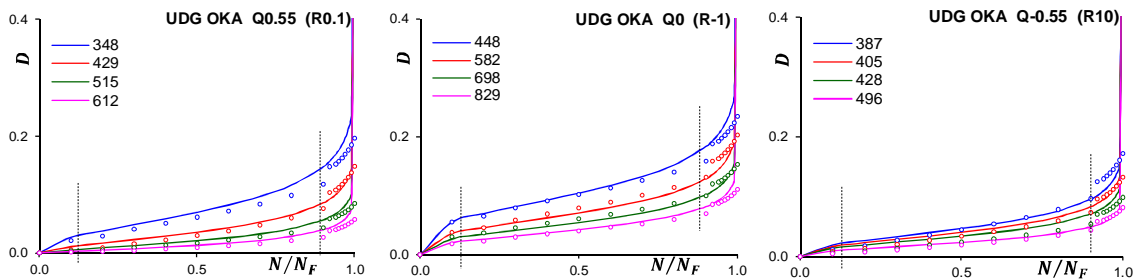


Figure 14 Non-linear damage evolution for rest material configurations (left) $R=0.1$, (middle) $R=-1$, (right) $R=10$ (legend shows $\Delta\sigma$ value in MPa)

The MAPE error metric value, more closer to 100%, shows that the final fatigue life predicted using CDM framework is more accurate than Multislope CLD model.

3.4. Fatigue testing on Glare FML panel containing transition to full-GFRP composite (ACASIAS project WP5 “Smart FML Panel”)

Joao de Freitas, Herman de Frel, Jan Waleson, Cees van Hengel (GKN Fokker), Petr Homola (VZLU, Prague, CZ)

In the framework of the European H2020 project ACASIAS, developments were done in WP5 “Smart Glare Panel” by GKN - Fokker Aerostructures (FAE), Fokker Elmo, NLR and VZLU (Prague, CZ) to develop FML panels with integral antennas. The aim is to integrate antennas into fuselage panels in order to reduce the aerodynamic drag and damage sensitivity of the conventional protruding antennas. In support of the panel design, a Mechanical Fatigue Testing (MFT) campaign has been performed on Glare Structural Element test samples (Figure 15). The samples were designed and manufactured by FAE, and tested by VZLU.

The test specimens consisted of a 1.4mm thick Glare3-3/2-0.3 region at the clamping area, which is representative of the basic skin (cyan color in Figure 15, and a center Glass Fiber Reinforced Polymer (GFRP) area (orange color in Figure 15) that was 3.5mm thick. In between those areas, a transition region (green color in Figure 15) included two interlaminar doublers to increase the Glare laminate thickness; this transition region also contains two 2.4mm rivet holes for electrical purposes. The GFRP region was designed such that the membrane hoop and shear stiffness values were similar to the Glare3 baseline material.

Fatigue tests were performed at VZLU to determine an S-N curve and to identify any potential fatigue-critical locations in the transition area. This campaign included tests on pristine and damaged (20J impact energy level on the first ply drop - Figure 15) structural elements. Additionally, the specimens were tested in different ambient conditions, namely at Room Temperature Ambient (RTA) and at Hot Temperature Ambient (HTA@80°).

Despite the fact that there were multiple test variables and conditions and few repeat samples, a global logarithmic trendline could be found (plotted in Figure 16), showing a coefficient of determination of $R=0.93$. All fatigue failures occurred at the stress concentration edges: at first plydrop (*i.e.* at the edge of the first internal doubler) or at the grip edge, indicating that neither the transition area nor the GFRP area were the weakest part in the design and also that the holes were not critical under fatigue conditions (Figure 17). Residual strength tests of the non-failed fatigued specimens (*i.e.* runouts) were performed and showed residual strength values that ranged from 520 to 660 MPa. Figure 19 show some representative examples of failed specimens. Figure 20 displays a failure sequence, within a 0.083ms timeframe, captured by a high speed camera.

The final test was on a dogbone-shaped large panel (external dimensions: 1200 x 760 mm including tapered tabs) containing two impact damages (Figure 21). For this test, a fatigue spectrum simulating hoop stresses was also applied (S_{max} 120 MPa, $R=0.1$, 1Hz, 180 kcycles, test at RTA, unaged) but no cracks initiated. A residual strength test was performed after cutting a 90 mm notch (saw cut) along the rivet-line. The failure occurred at 450 kN at a gross failure stress (relative to the undisturbed Glare 3-3/2 area: 740mm wide and 1.4mm thick) of 434 MPa. The failure mode was a stable damage extension from one of the notch tips (Figure 22).

In conclusion, the test program has shown that a pure Glass-Epoxy “patch” can be created in a Glare FML laminate in a straightforward way with good mechanical properties.

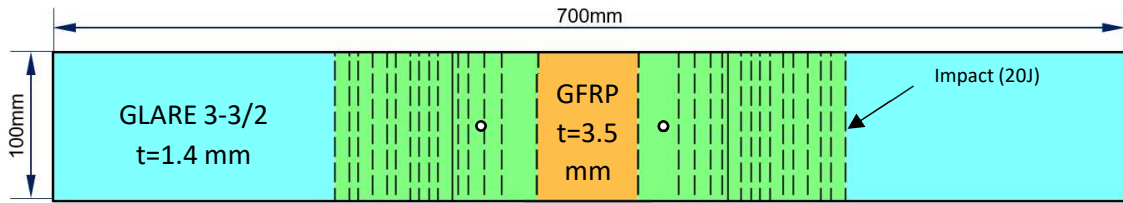


Figure 15. Structural element test specimen with two 2.4mm holes: drawing showing material regions and plydrop locations.

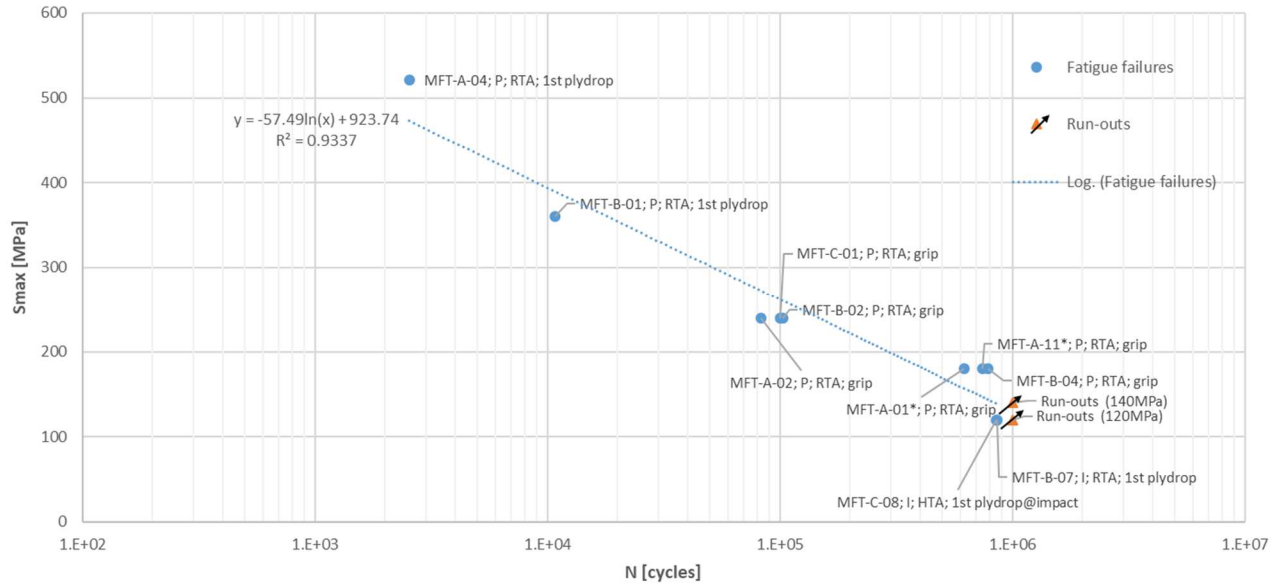


Figure 16. S-N curve for structural element MFT to failure.

Note: S_{max} in the thinnest cross section (Glare 3-3/2-0.3, $t=1.4$ mm, $w=740$ mm) is used as the stress reference. Label code: Specimen number; damage status; ambient conditions; failure location.



Figure 17. Failed MFT-A-04 specimen with intact crack wires positioned at 1mm from the hole edge.

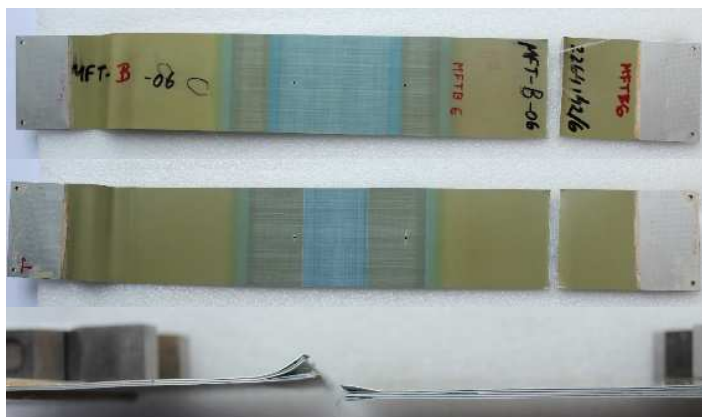


Figure 18. Failed MFT-B-06 specimen; pristine and tested in HTA for fatigue and RTA for the residual strength test: IML view (top), OML view (middle) and side view detail of the failure region (bottom).



Figure 19. Failed MFT-C-06 specimen; impacted (20J) and tested in RTA: IML view (top), OML view (middle) and side view detail of the failure region (bottom).

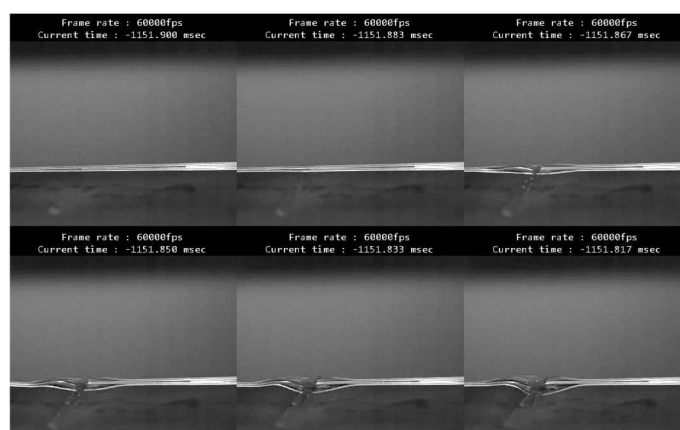


Figure 20. High speed camera video sequence showing the moment of failure initiation. Frame rate of 60 000 fps.

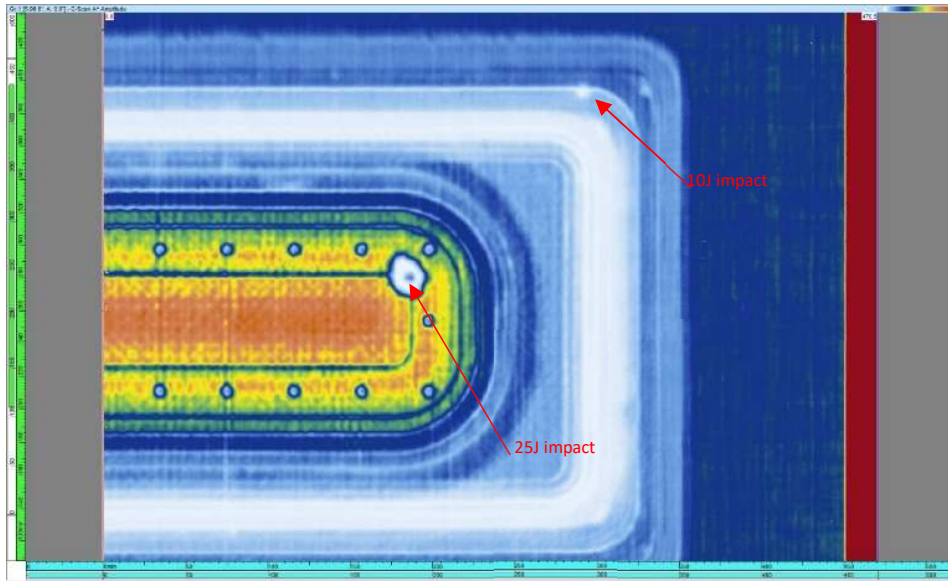


Figure 21. C-scan image after damage application and before the pre-fatigue measurements (@VZLU).

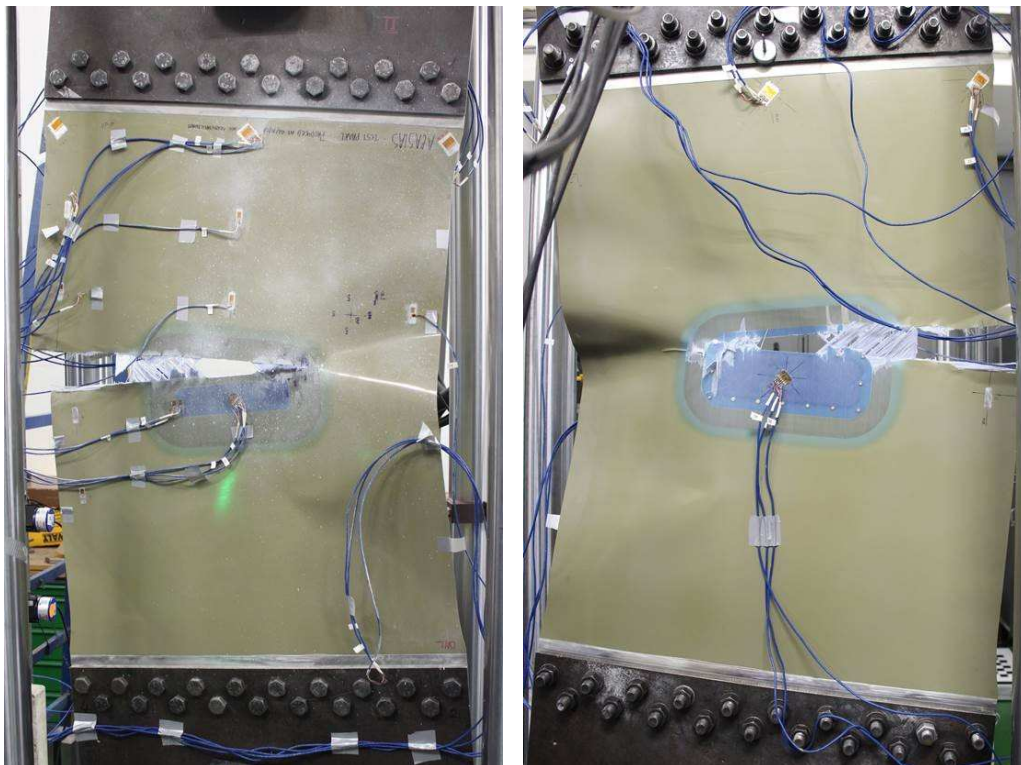


Figure 22. Failed panel after residual strength test. Failure occurred at the 90 mm long notch collinear with the rivet-line. OML view (left); IML view (right)

3.5. Residual strength of impact damage in skin and skin-stringer interface in thermoplastic orthogrid fuselage panels

J.E.A. Waleson, J.W. van Ingen (GKN Fokker)

In 2013, Fokker Aerostructures developed a new stiffened skin panel concept for fuselages. The concept features frames that are welded to an orthogrid stiffening structure, thus eliminating a large number of mechanical fasteners. The concept is made possible by “butt joining” the stiffener webs to a skin laminate and melting them together [17].

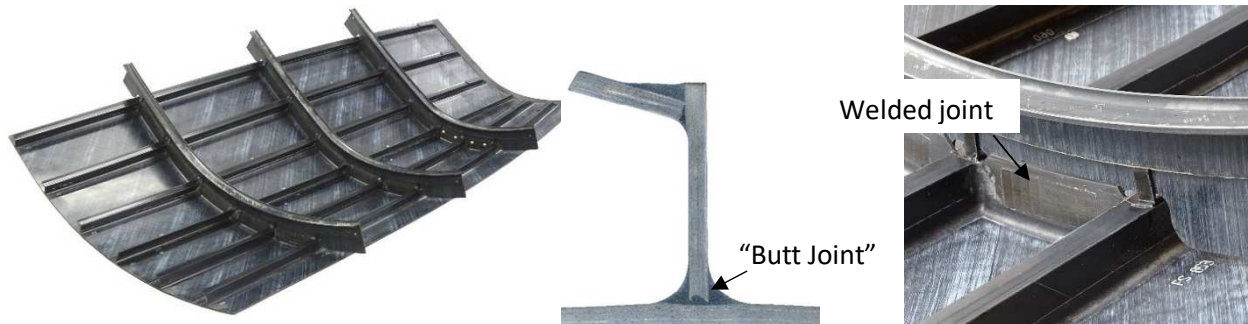


Figure 23 New stiffened fuselage panel concept without mechanical fasteners.

A critical aspect for certification is showing sufficient residual strength of Barely Visible Impact Damage in the skin-to-stringer butt joint caused by tool drop on the inside of the fuselage. An ABAQUS VCCT analysis supported by test was developed with TU Delft, see Figure 24.



Figure 24 Test panel with a delamination in the skin – middle stringer interface representing Barely Visible Impact Damage.

Residual strength of the butt joint damage was tested on three-stringer panels loaded in compression. Good correlation of the load displacement curve and failure load in analysis and test was shown in [18].

Another damage tolerance aspect is the residual strength of obvious damage, which can be found within a few flights. In [19] and [20] it is referred to as category-3 impact damage. It also shows that there is no cliff in the residual strength curve beyond the impact damage from the smaller impactor diameters that are commonly used in the impact test programs for Barely Visible Impact Damage (category 1) and Visible Impact Damage (category 2). The extent of the damage was determined by an indentation of a 3-in diameter sphere on flat 3-stringer panels to cover impacts between the frames and, to cover impacts at the frame locations, on a double curved panel with boundary conditions approaching those in a fuselage.

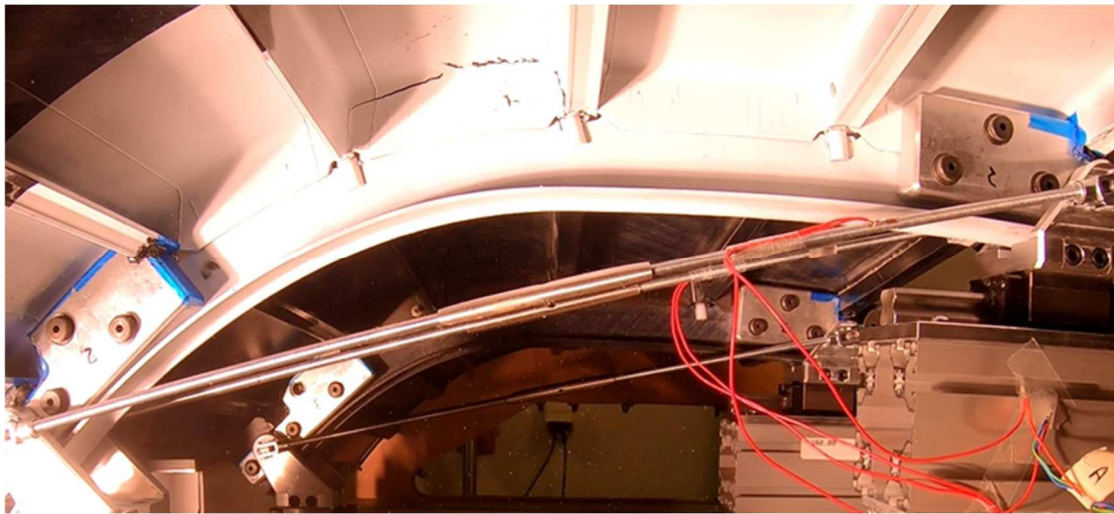


Figure 25 Double curved test panel with boundary conditions approaching those in a fuselage used to test obvious damage.

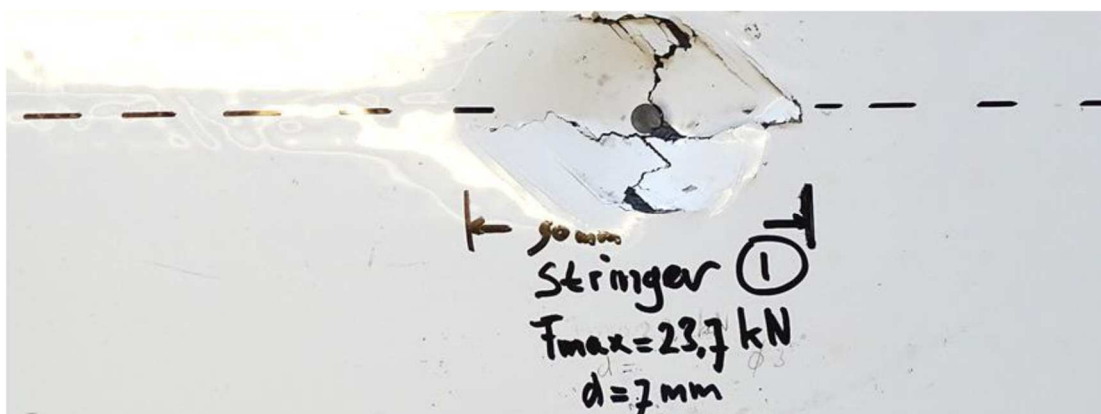


Figure 26 Test panel with obvious impact damage at a stringer (delaminated within the frame bay) between the frames.

A stringer separated from the skin within one frame bay combined with a 100-mm skin crack in circumferential direction was considered critical for an unpressurized fuselage keel panel at fuselage downbending. A point strain analysis method developed with NSE Composites was used to predict

the panel load at onset of damage growth in the skin laminate. Figure 5 shows the ABAQUS model used in the point strain analysis. Note that the disbonded segment of the stringer was omitted from the model to account for damage to the stringer at the impact location. The analysis showed sufficient residual strength.

Arrest of the crack in the skin at adjacent stringers is part of current investigations.

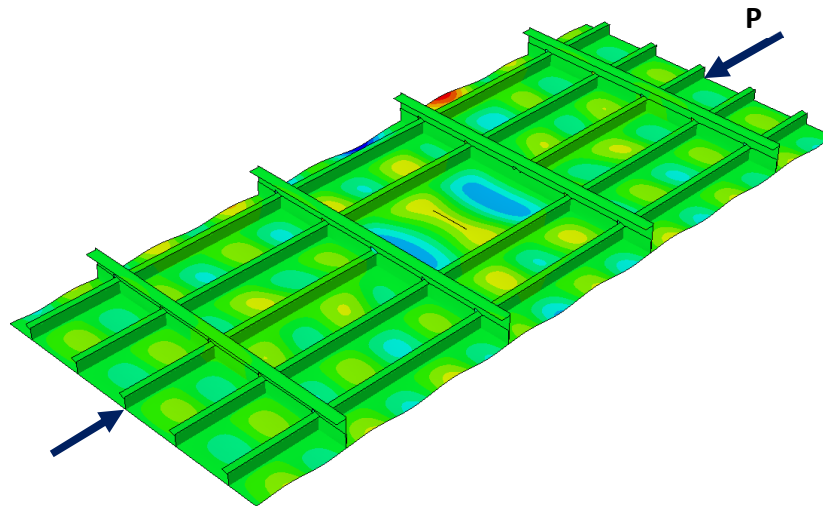


Figure 27 ABAQUS model to predict onset of damage growth through the skin laminate by means of a point strain method.

3.6. Characterization of delamination onset and propagation under fatigue loading of AS4D/PEKK-FC thermoplastic composites

Bas H.A.H. Tijs (GKN Fokker, TUDelft), Jordi Renart, Albert Turon (AMADE, University of Girona).

The use of thermoplastic composites materials is gaining momentum in the transportation sector due to their improved mechanical properties, "unlimited" shelf life and to the fact they offer a number of advantages that can benefit cost-efficient and high-volume manufacturing. However, the amount of work in literature on the mechanical behaviour of thermoplastic composites under cyclic loading is rather limited. In this work, an experimental test campaign to characterize the interlaminar behaviour of a thermoplastic material under fatigue loading is presented.

The material used in this study is the Solvay (formerly Cytec) APC(PEKK-FC) thermoplastic polymer prepreg which consists of a fast crystalizing thermoplastic matrix of poly ether-ketone-ketone commonly referred to as PEKK-FC, reinforced with the continuous unidirectional AS4D fiber. A AS4D/PEKK-FC laminate that consists of 30 unidirectional plies was manufactured through auto-clave consolidation and specimens for both mode I and II fatigue tests were machined. The specimens were designed to be 25mm wide and 225mm long in order to accommodate for sufficient room to achieve stable crack propagation during mode I and II testing. Due to the high melting temperature of thermoplastic composites, a 12.5 micron thick UPILEX foil (60mm long) was used as insert to start the crack.

Taking advantage of the multi-specimen test rig developed at the AMADE research lab [21], series of six specimens have been tested in parallel at different load levels to obtain the fatigue curve for delamination onset. The tests have been initially performed from the insert, without creating any

initial pre-crack. In Figure 28, the onset curves obtained from the insert, without the creation of a precrack are shown. After the first round of fatigue tests, static tests have been run to all the specimens to create a pre-crack and ensure similar conditions for the crack front. Afterwards, the two series of fatigue tests have been repeated. The same procedure has been applied to obtain the propagation curves (crack growth rate versus applied maximum energy release rate curves).

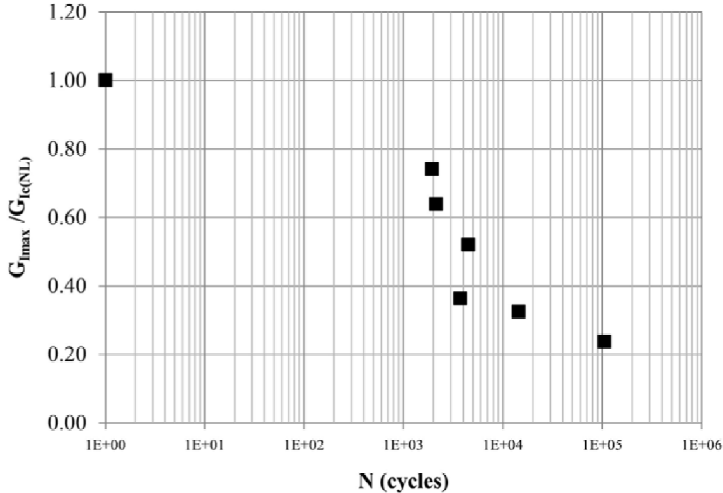


Figure 28 Fatigue life curves for onset of delamination (5% increase in compliance) under mode I loading from specimens without an initial pre-crack.



Figure 29 Multi-specimen test rig used to characterize the fatigue behaviour under mode II loading.

Under mode II loading, a new multi-specimen test rig has been designed (see Figure 29). In this case, 4 specimens are loaded in parallel using an MMB fixture [22]. The level arm has been selected for a 98% of mode II. This new multi-specimen test rig is used to run series of fatigue tests and obtain the fatigue curves for delamination onset. The same procedure has been applied to obtain the propagation curves, but in this case, a compliance calibration of the specimens before and after the test is done. The influence of the initial state of the crack front and the loading mode were analysed and discussed.

3.7. Unfolding the Early Fatigue Damage Process for CFRP Cross-Ply Laminates

Xi Li, Rinze Benedictus, Dimitrios Zarouchas (TU Delft)

Early fatigue damage usually refers to damage within the first 10% of the fatigue life that is distributed throughout the entire laminate leading to stiffness degradation and specimen heating. As it is matrix-dominant, it contains two mechanisms: off-axis matrix cracks and delamination. For coupon-level laminates, off-axis matrix cracks usually generate at free edges due to stress concentration, which then propagate through the fibre direction [23,24]. Considering randomly-distributed micro-defects, such as voids, inclusion of foreign particles and local fibre-matrix debonding, which usually occurs during the manufacturing process, the resistance to off-axis matrix cracks under fatigue loading varies among local regions of a laminate [25]. As a result, the fatigue life, when the first off-axis matrix crack occurs, usually presents a significant scatter band, especially for low stress levels [26]. During the subsequent fatigue cycles, the number of off-axis matrix cracks gradually increases up to a saturation state, which is also termed as Characteristic Damage State (CDS).

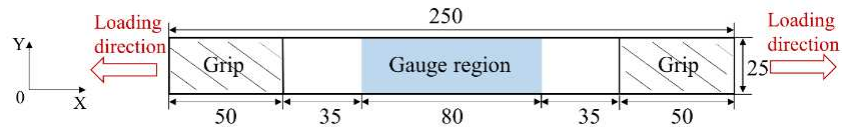
Experimental evidences showed that both fatigue life and matrix crack density at CDS depend on stress levels and loading control modes, and they can be even different among nominal identical specimens subjected to the same loading conditions. Delamination is another damage mechanism that appears at the early fatigue life of a laminate and it usually originates from the tips of off-axis matrix cracks or free edges due to the high inter-laminar stress concentration. Initially, it was hypothesized that, delamination initiates after CDS, however, experimental observations showed that before reaching CDS, delamination may appear specifically at regions with high density of off-axis matrix cracks. Both damages contribute to significant stiffness degradation which appears within a short duration of fatigue life.

This study investigated the early fatigue damage of cross-ply carbon/epoxy laminates. The aim was to unfold the damage accumulation process, understand the interaction between different damage mechanisms, and quantify their contribution to stiffness degradation. Rectangular shape specimens with 250 mm × 25 mm size and stacking sequence of $[0_2/90_4]_s$ were fabricated using unidirectional (UD) Prepreg named Hexply® F6376C-HTS(12K)-5-35% with high tenacity carbon fibres (Tenax®-E-HTS45) and a tough epoxy matrix (Hexply® 6376), Figure 30 (a).

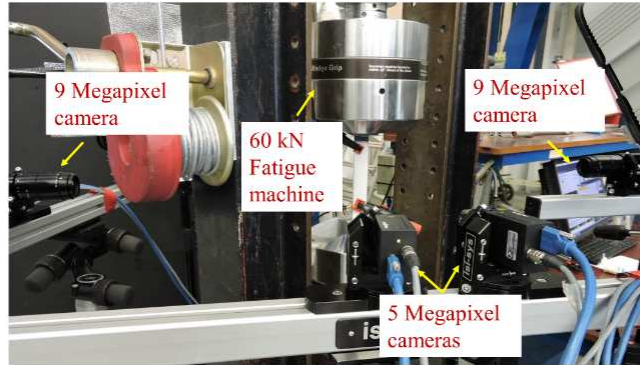
The specimens were tested under tension-tension fatigue loading on a 60 kN hydraulic fatigue machine at room temperature. The test set-up and a schematic representation of applied loading profile, containing the repetitive cyclic loading blocks and the tensile loading-unloading ramps, are shown in Figure 30 (b) and (c), respectively. Constant amplitude of sinusoidal waves, with maximum stress of 507 MPa (70% of UTS), stress ratio 0.1 and frequency 5 Hz were applied, while the tensile loading and unloading ramps were applied before and after every 500 cycles with the rate of 19 kN/s.

The main conclusions are listed here after:

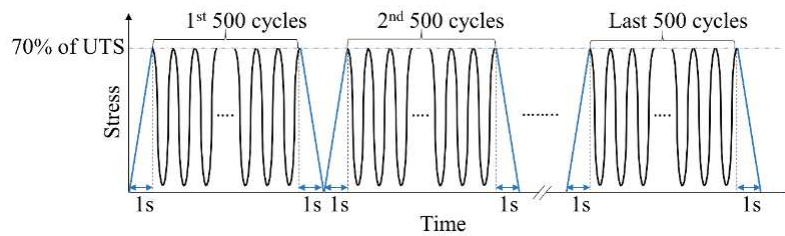
- Until the end of Stage I, stiffness degrades about 8% to 11% and two groups of decreasing trends are obtained among specimens, see Figure 31.
- For specimens where stiffness degrades slower, both damage mechanisms also show relatively slower growth rates and longer fatigue life is consumed to reach CDS, see Figure 32.



(a)



(b)



(c)

Figure 30 The schematic diagram of specimen dimensions, gauge region and clamping area (in [mm]), and loading direction (a); Test set-ups (b); Loading pattern of fatigue test (c) [27].

Delamination is responsible for larger stiffness degradation than transverse matrix cracks at Stage I. This observation is attributed to the ply-block of 90° plies. A linear increase of stiffness degradation is obtained with the increase of matrix crack density, while the growing trend of stiffness degradation due to delamination converges with the increase of delamination ratio, see Figure 33. Further details of this work can be found in [27].

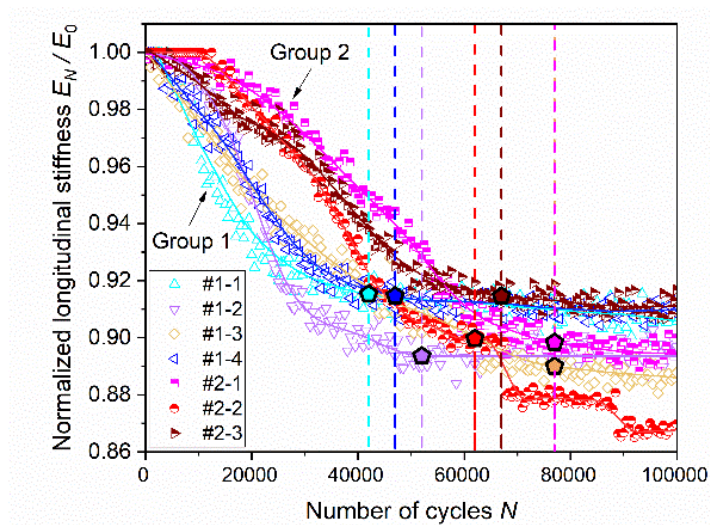


Figure 31 Normalized longitudinal stiffness versus number of cycles for cross-ply laminates within 10^5 cycles [27].

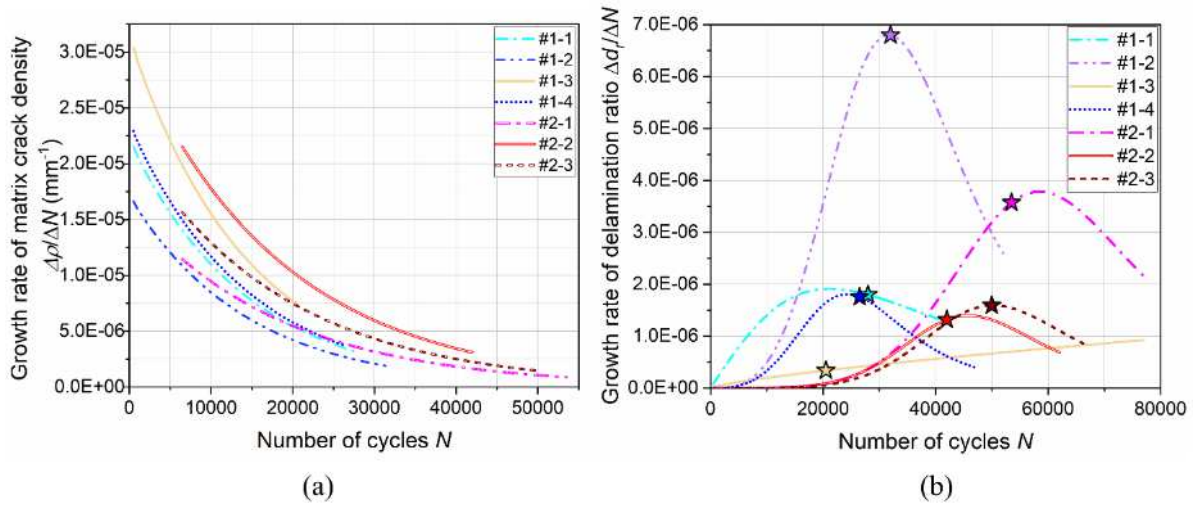


Figure 32 The growth rate of matrix crack density (a) and delamination ratio (b) with the increase of fatigue life [27].

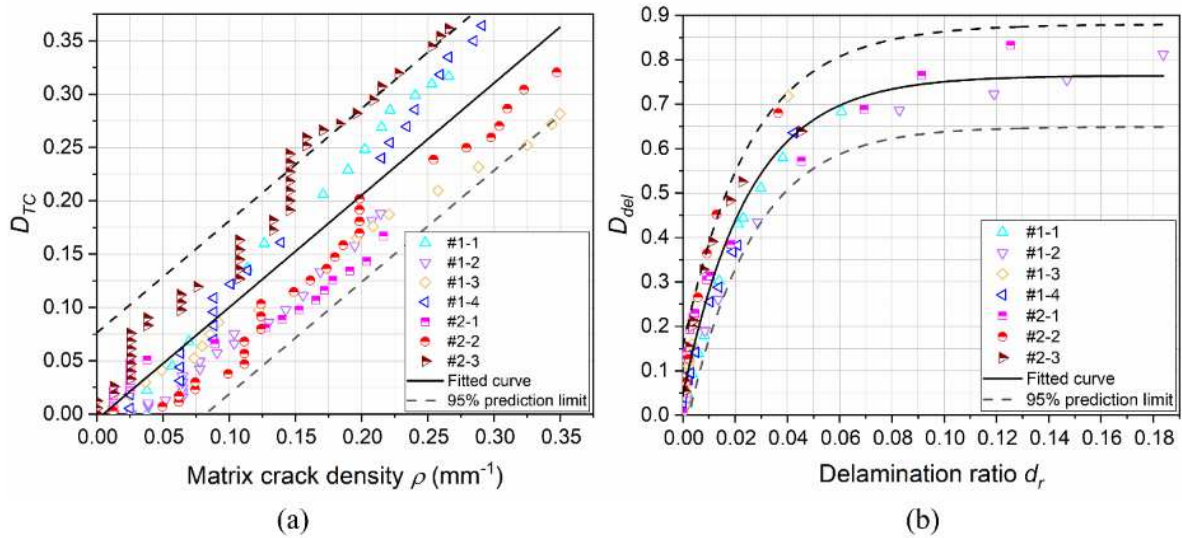


Figure 33 The plots of normalized stiffness degradation contributed by transverse matrix cracks with matrix crack density (a); the plots of normalized stiffness degradation contributed by delamination with delamination ratio (b) [27].

4. Prognostics & Risk Analysis

4.1. Adaptive Prognostics for Remaining Useful life of Composite Structures

Nick Eleftheroglou, Dimitrios Zarouchas, Rinze Benedictus (TU Delft)

The field of prognostics aims at supplying reliable predictions for the future state of a system based on up-to-date information by incorporating monitoring data, machine learning algorithms, the physics of the systems' degradation and reliability analysis. The engineers target at converting these predictions to information and make decisions on the future use of the system, where one main output could be the remaining useful life (RUL) of the system [28].

Recently, prognostics of composite structures has become a dynamically rising field of research. The main target is to estimate the remaining useful life in real-time of the composite structure while it is in service. The degradation process of a composite structure is a nonlinear and time-varying dynamic process of stochastic nature. Composite structures usually operate in non-uniform environments and altering operational conditions e.g. loads, whereby data are changing. The composite structure's life is heavily influenced by the way it is operated, maintained, the environmental and operation conditions, which are not always the designed ones, because unexpected phenomena may occur during the structure's lifetime. For the latter, let's consider an example from the aviation industry.

Foreign objects impacts, such as bird-strikes, hail, tool drops etc., may occur anytime during the lifetime of the aircraft. These events fall into category of accidental (unexpected) phenomena that may create damage, which may have not been anticipated into the design phase. The implication of such an unexpected event to the integrity of the structural component could be severe and a common practice, as long as the operators record the event, is to interrupt the aircraft operation and initiate inspection and repair actions resulting to unplanned costs. In this case, the role of a RUL prediction approach would be to assess the effect of the unexpected event and to provide an updated prediction.

This study proposes a new data-driven prognostic approach, which is an extension of the Non-Homogenous Hidden Semi Markov Model (NHHSMM) [28-30]. The proposed model is capable of real-time learning and adapting the estimated model parameters based on the availability of real-time data [31,32]. Figure 34 presents the dynamic adaptation process. In the present paper, similar fatigue tests were executed on open-hole quasi-isotropic

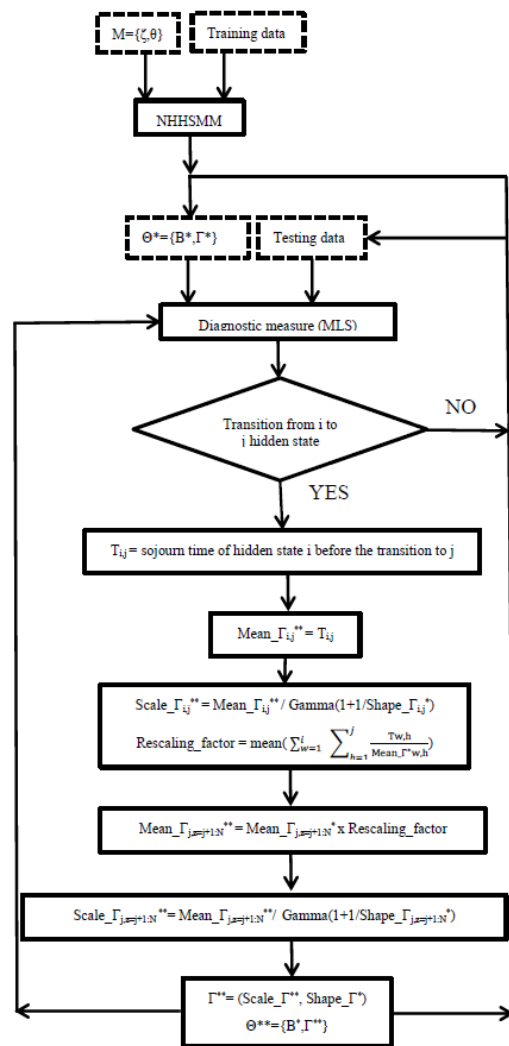


Figure 34 Dynamic adaptation process

specimens and in addition, in order to simulate an unexpected phenomenon, in-situ impact took place during the fatigue loading.

To demonstrate the adaptability and the efficiency of the proposed approach, open-hole carbon/epoxy specimens with stacking sequence $[0, \pm 45, 90]_{2s}$ were subjected to in-situ impact and constant amplitude fatigue loading up to failure; Figure 35 presents the experimental set-up. The training data set consists of health monitoring data collected from specimens, see Figure 36 specimens with bold lines, which were subjected only to fatigue loading, while the testing data set consists of health monitoring data collected from specimens which were subjected to fatigue and in-situ impact loading, see Figure 36 specimens with dashed lines. The impact loading was introduced only to the testing process aiming to influence the fatigue life and produce outlier cases. In that case, the in-situ impact can be considered as an unexpected phenomenon and unseen event regarding the training process.



Figure 35 The experimental set-up

Figure 36 presents the Weibull pdfs which are shifted to the left side as it was desired since specimen10 is the left outlier. In this direction the ANHHSMM prognostic estimations are expected to be more accurate, comparing with the NHHSM estimation since the mean sojourn time values are getting shorter, see Figure 37. Further details of this work can be found in [31,32].

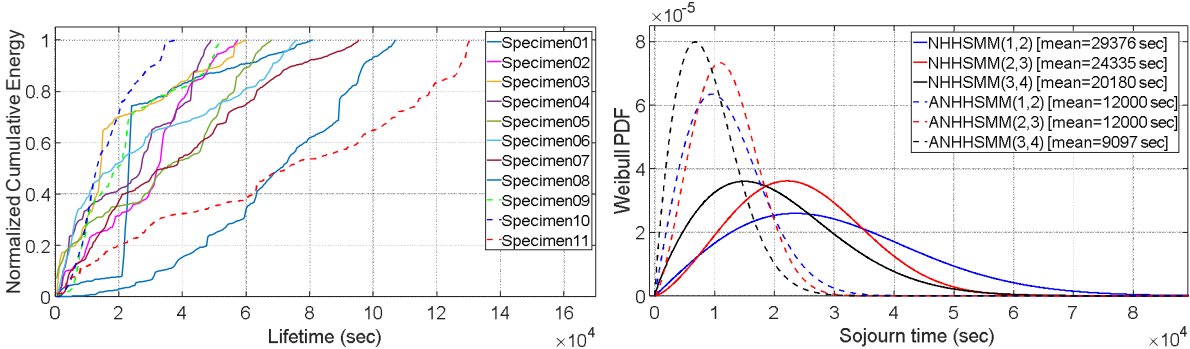


Figure 36 Normalized cumulative AE energy observation histories and adapted sojourn time Weibull distributions for specimen 10

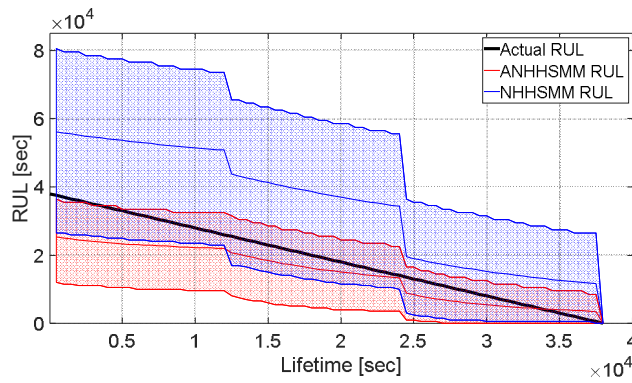


Figure 37 RUL predictions of the left outlier (Specimen10)

4.2. Probabilistic Fail-Safe structural risk analyses

F.P. Grooteman (NLR)

Most aircraft are designed according to the damage tolerance philosophy. This may be done in a deterministic way or a probabilistic damage tolerance analysis may be performed: a so-called structural risk analysis (SRA) – see Figure 38. An SRA takes into account all important scatter sources, such as the initial flaw size, the inspection quality, the variability in loads and crack growth material properties. For new military aircraft, SRA is mandatory as prescribed in MIL-STD-1530D and MIL-STD-882E. For current aircraft, it already has become a valuable tool for fleet management, since it offers a risk (probability of failure) development over time, which cannot be obtained from the traditional deterministic damage tolerance analysis. It provides fleet management information when to take corrective actions.

Currently SRA is applied to single load path structures only. Many aircraft structures however have multiple load paths, where after a (partial) failure of a load path the remaining structure can sustain limit load. Such a multiple load path structure can be analysed by a so-called damage tolerance Fail-Safe analysis, which often results in a very conservative inspection scheme. The possibility that the crack can start in any of the load paths with a size that is much better represented by a distribution function than by some upper bound value, demands for a probabilistic approach. For this, a new probabilistic Fail-Safe approach has been developed, see Figure 39. The approach is an extension of the single load path SRA. The methodology has been implemented in the NLR in-house tool SLAP++ (Stochastic Life Approach). This tool also provides functionality to support the generation of the necessary structural risk analysis input. The new probabilistic Fail-Safe approach was demonstrated with a realistic example and compared against the deterministic Fail-Safe approach [33], demonstrating the high level of conservatism of the deterministic Fail-Safe method, yielding mostly redundant inspections. By application of a probabilistic Fail-Safe analysis, the number of inspections and related down-time can tremendously be reduced together with a demonstrated increase in the remaining useful life of the structure, especially when an NDI technique is applied in order to find cracks long before an expensive failure of the primary load path or in cases where a simple visual inspection does not apply.

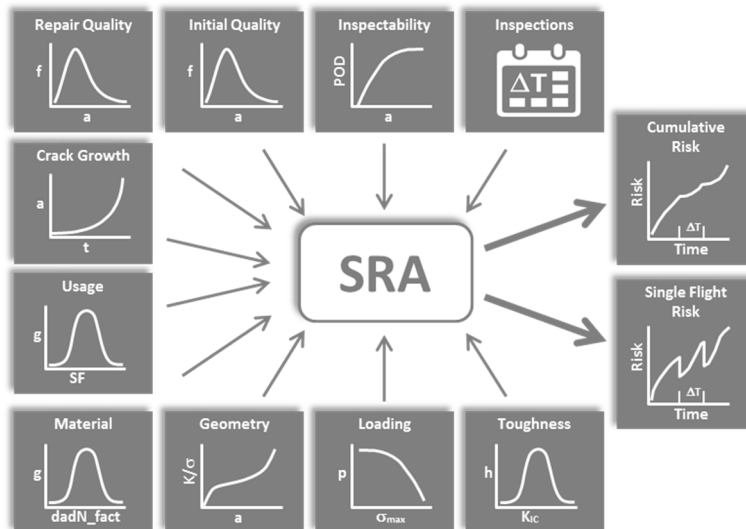


Figure 38 Schematised structural risk analysis.

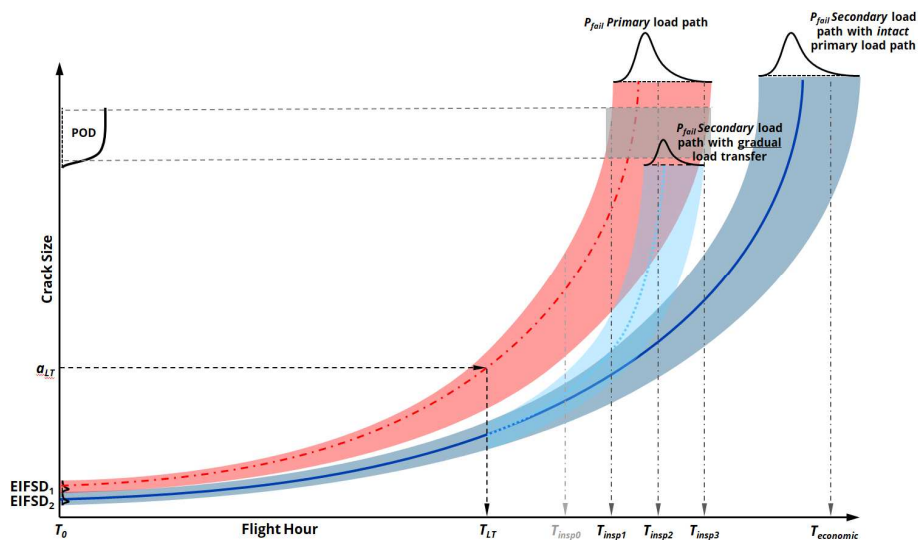


Figure 39 Schematized probabilistic Fail-Safe analysis

4.3. Predicting helicopter damage caused by a collision with an Unmanned Aerial System using explicit Finite Element Analysis

Michiel Schuurman, Boyang Chen (TU Delft), Laurens Jonkheim (RNLAf)

Due to an exponential growth in the number of shipments of Unmanned Aerial Systems (UAS), the amount of these devices operating in the sky has increased remarkably over the last few years. This led to an increasing number of proximity incidents with manned aircraft. Since these devices share certain airspace with rotorcraft, the question arises how much damage a helicopter could sustain after an impact with a UAS. Within this thesis, a risk assessment was completed initially to determine which collision in terms of type of UAS and helicopter impact location poses the highest risk to the operator of the helicopter. Subsequently a validated model of a DJI Phantom III was developed and impacted onto a rotorcraft windshield in explicit Finite

Element software. The sustained damage was compared with a simulated bird strike event to determine whether the prevailing certification requirements would suffice to guarantee safety of the crew.

Table 1 Risk matrix helicopter impact location based on frontal size

		Effect		
		Negligible	Moderate	Catastrophic
Chance	Probable			Main rotor blade
	Possible	Fuselage skin	Windsheld	
	Improbable		Engtne inlet Horizontal tailplane Vertical tailplane Landing gear	Tail rotor blade Rotor mast



Figure 40 Agusta A-109 CAD model (GrabCAD, 2014).

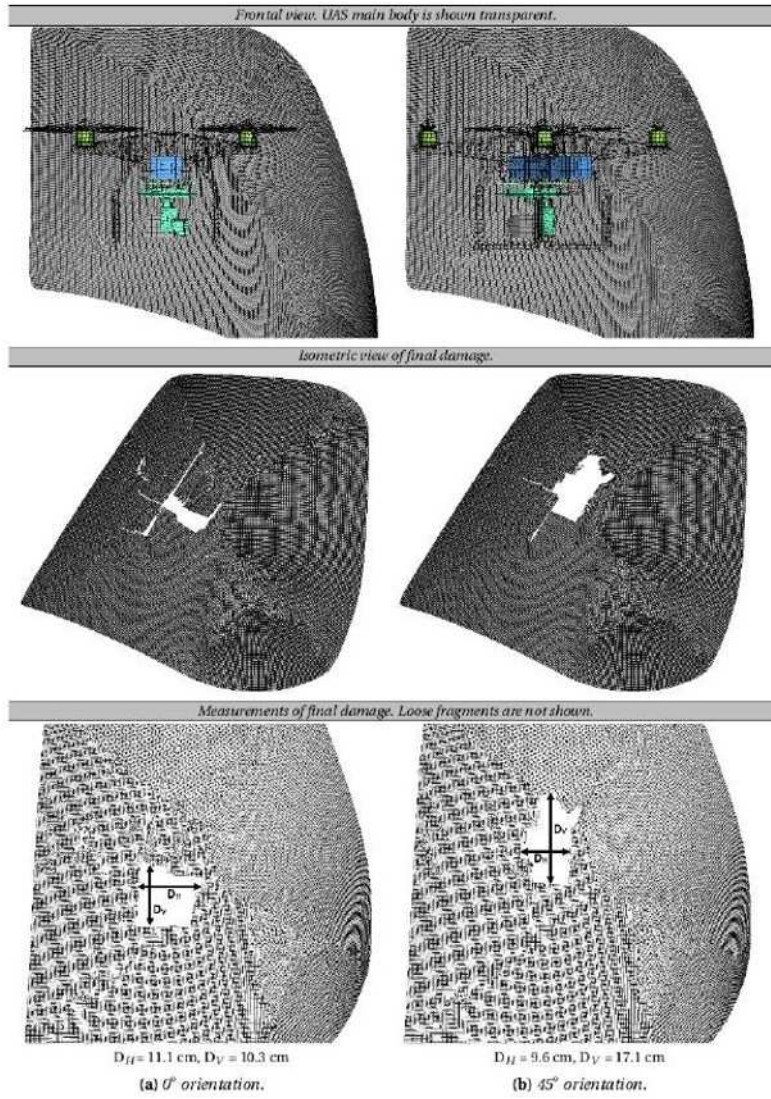


Figure 41 Comparison of the damage of a 14.0 mm thick windshield impacted by the UAS for various UAS orientations

5. Non-Destructive Evaluation

5.1. Load monitoring of cantilever structures using a single optical fibre

Nakash Nazeer and Roger M. Groves (TU Delft)

In this research, a novel fibre optic sensing methodology is developed with the aim of monitoring the loads on cantilever structures. The first part of the study deals with a simple cantilever beam that undergoes pure bending. The second part deals with a complex cantilever plate that includes both bending and twisting. This is then extended to aircraft wings for the purpose of shape sensing and load monitoring.

The sensing fibre for this purpose makes use of fibre Bragg grating (FBG) sensors. The fibre is also designed such that it doesn't contain a large array of gratings or involve complex and intricate manufacturing procedures such as multi-core fibres. Another condition put in place was to use least number of (grating) sensors for load monitoring. This was incorporated in efforts to reduce to the cost of the sensing fibre and to study the minimum number of sensors required to achieve the load monitoring goal. On the other hand, this condition poses a drawback. By reducing the number of gratings, the amount of data acquired would also reduce. To tackle this, two principles of optical fibre sensing were utilised such that additional data could be captured while keeping the number of gratings at a minimum.

The sensing technology and algorithm developed here uses a method of incorporating both hybrid interferometry and FBG spectral sensing. When the fibres, and in turn the gratings, are subjected to external (mechanical and/or thermal) disturbances two optical phenomena occur. The first one corresponds to the spectral shift of the Bragg wavelength ($\Delta\lambda_B$) of each grating and is represented as a change in strain ($\Delta\varepsilon$) as:

$$\Delta\varepsilon = \frac{\Delta\lambda_B}{\lambda_B(1-\rho_\alpha)} - \Delta T \left(\alpha_n + \frac{\xi}{(1-\rho_\alpha)} \right) \quad (1)$$

where ΔT is the change in ambient temperature, ρ_α is the photo-elastic coefficient, α is the thermal expansion coefficient and ξ is the thermo-optic coefficient.

The second is the change in optical distance between any two gratings. This follows the Fabry-Pérot principle which is based on multiple wave interferences between two partially reflecting mirrors. In our case, we considered each grating as a mirror and the distance between any two gratings as a long Fabry-Pérot cavity. This change is recorded as strain (ε) as is represented as:

$$\varepsilon = \frac{\Delta l - L_t \Delta T}{L} \quad (2)$$

where Δl is the change in cavity length, L is the original cavity length and L_t is the change in cavity length due to change in temperature.

For a cantilever beam it was demonstrated that a single fibre containing two FBGs was sufficient to simultaneously measure the location and magnitude of external loads. This information was also used to capture the deformed shape of the beam. These findings were presented at the 2019 SPIE Smart Structures + Nondestructive Evaluation conference in Denver, USA [34].

On the other hand, for cantilever plates, it was demonstrated that a single fibre with four FBGs was sufficient to measure the location and magnitude of external loads [35]. The plate could be considered

as two beams stitched to each other. This way both bending and twisting could be captured. Figure 42 shows the setup used to run the experiments on the cantilever plate. Figure 43 shows examples of the estimation of the loading position and magnitude at two different locations on the plate. The estimation achieves a maximum error of 9% on a 1 m x 1 m plate. The data acquired can be mapped on the surface to help retrieve the deformed shape of the entire structure. This fibre-optic sensing methodology can also be incorporated in composite structures given the unobtrusive nature of optical fibres. When it comes to aero applications, this data acquired can be integrated with the control loop for real-time feedback for load monitoring and load alleviation purposes.

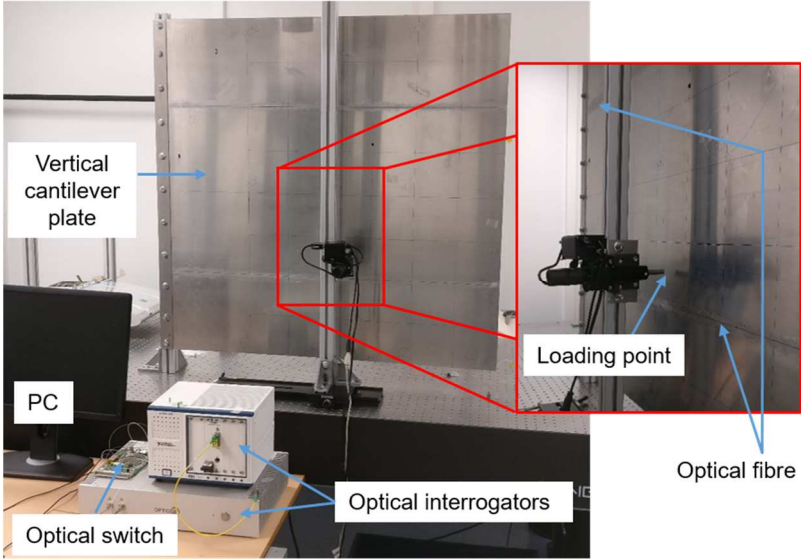


Figure 42 Lab setup for the cantilever plate experiments.

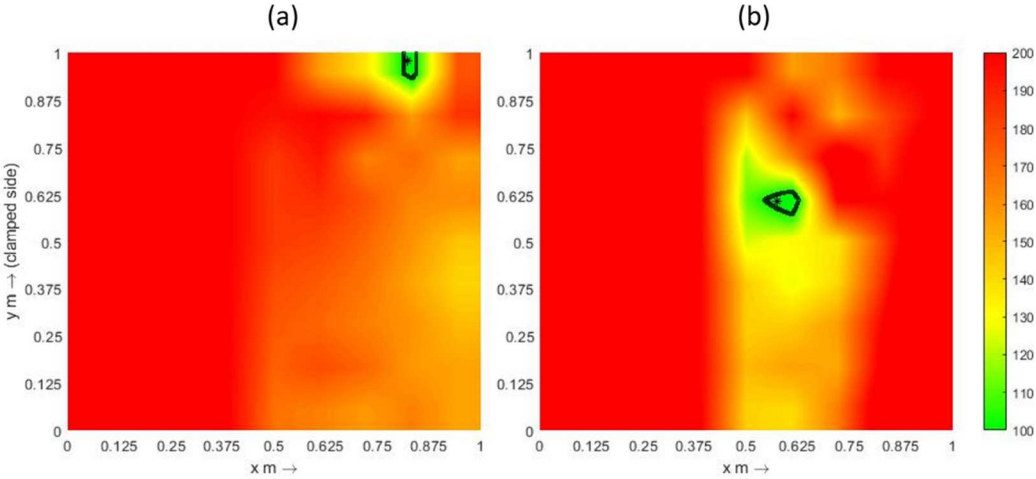


Figure 43 Estimation of location and magnitude of (a) corner load and (b) centre load. On the colour-map, 100 corresponds do the exact loading position.

5.2. Automatic fusion of different Non-Destructive Inspection techniques

Jason Hwang, Patrick Jansen, Jacco Platenkamp (NLR)

Non-Destructive Inspection (NDI) of structural components is an essential activity to ensure the airworthiness of flight critical components. Various techniques are available for this purpose, each with its own merits. In a feasibility study, NLR has explored the possibility and benefits of integrating a number of available NDI technologies, including novel visual techniques – see Figure 44, to obtain an efficient and effective way for quickly inspecting critical components such as wing flaps or helicopter rotor blades. By fusing the resulting data and automatically stitching the different frames, a comprehensive and yet easy-to-understand picture is obtained that provides the maintainer with accurate information regarding the condition and geometric properties of the inspected component.



Photogrammetry



3D structured light scanning



Thermography



Shearography

Figure 44 Overview of the different techniques applied to a flap of a Boeing 747 aircraft.

A particular application that has been considered was the inspection of helicopter rotor blades. A combination of different NDI techniques was applied to rotor blade segments that contained artificial defects and to full-scale rotor blades that contained repairs. It was shown that the geometrical properties of a full-scale blade can be accurately measured and compared to a reference condition. Also, it was demonstrated that the combination of automated thermography and shearography inspections could replace a significant part of the manual inspection burden as mandated by the maintenance manual. By combining multiple scan data, artificial damages inserted in the reference test specimen, in-service repairs and impact damages could be found and graphically presented to the maintainer. Furthermore, it was demonstrated that 3D structured light scanning can be used to detect external geometrical features such as holes, erosion, impacts and large surface repairs. Additionally, 3D structured light scanning provides a 3D surface mesh on which the multiple NDI data can be mapped and stitched onto, helping the maintainer in the interpretation of the data more easily and quickly, see Figure 45. An additional benefit is that the location and dimensions of defects can be easily and accurately extracted.

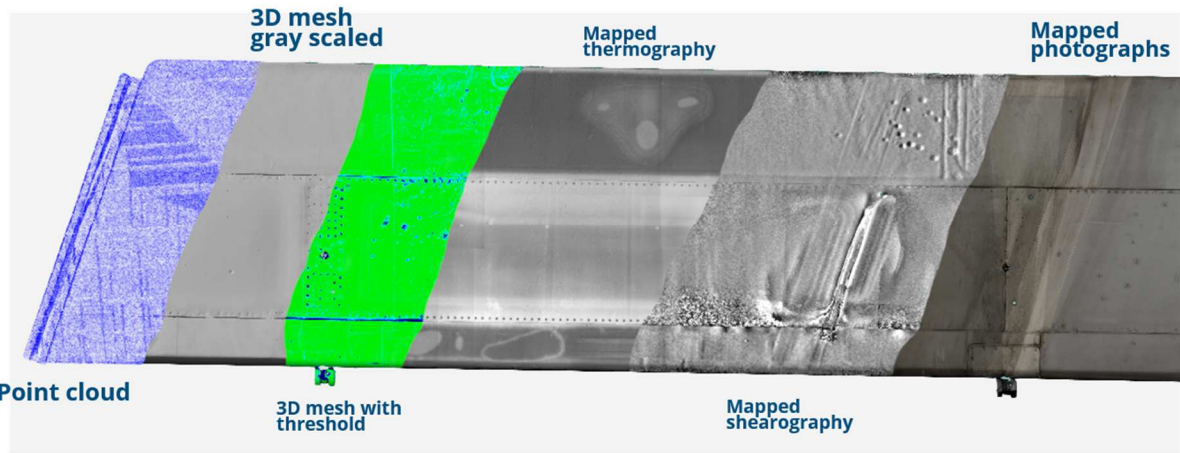


Figure 45 Overview of an inspection results, showing the mesh, surface defects, mapped visual photographs, mapped thermographic phase images and mapped shearographic image.

The next phase of is to build a full-scale automated demonstrator integrating these sensors. The objective is to further develop the system, automating the maintenance process in step-by-step development, collecting sufficient data from in-field to support validation of the method.

6. Structural Health & Usage Monitoring

6.1. Landing gear health monitoring

Frank Grooteman (NLR)

In the European Clean Sky 2 project ALGeSMo on Advanced Landing Gear Sensing & Monitoring, a state-of-the-art fibre optics-based load monitoring system has been developed and successfully demonstrated that measures the service loads at the landing gear wheels – see Figure 46 for a schematised overview of the whole system. In addition to health monitoring of the landing gear, the system can also be applied for accurate and rapid classification of hard landing and overload events, for determining braking moments, for accurately measuring the weight on wheels and centre-of-gravity position in an automated way, and for the reliable detection of air-ground transitions. The development consortium consisted of Meggitt (SA and UK), PhotonFirst (NL) and NLR (NL) together with Airbus (UK) as the topic leader.

The load monitoring system consists of a sensor with several Fibre Bragg Gratings (FBG) that can be retrofitted in the axle of the landing gear, a newly developed fibre optic processing unit to measure the optical fibre output, and all the optical cabling from the sensors to the processing unit including all connectors and harnessing. The whole system has successfully been demonstrated in a specially designed and built test rig at NLR in which loads could be applied in all directions at each wheel location including a braking moment, see Figure 47. In a several month-long test campaign the system has thoroughly been tested with loads representative of aircraft operation as specified by Airbus. The axle sensor was instrumented with conventional foil strain gauges and temperature sensors which compared very well with the FBG data. The tests consisted of calibration tests to provide data for the calibration of the axle sensors and then moved on to high-load tests, dynamic tests, tests at high and low temperatures, shock and vibration tests, etc. The outputs of the ALGeSMo system were continuously recorded and compared to the actually applied loads and the measurements of the strain gauges and temperature sensors.

The load measurement accuracy depends on many parameters (e.g. temperature, load amplitude, etc). The plots in Figure 48 show a representative example of the accuracy obtained during the tests. The axes are purposefully left blank in order not to disclose sensitive data. These plots show the accuracy (vertical axis, expressed as a percentage of the maximum load) depending on the load amplitude (horizontal axis). These are for vertical loads and for each side of the axle (there are two wheels per axle, hence two axle sensors). It can be seen that the accuracy is generally within the specified range (red dotted lines), with the exception of a few data points. This is representative of the overall results. Load measurement in some specific situations still can be improved.

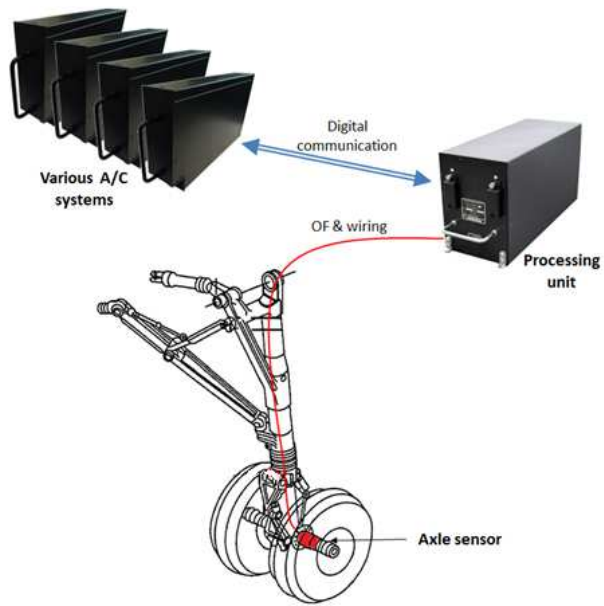


Figure 46 High-level ALGeSMo health monitoring system overview.



Figure 47 Landing gear health monitoring test bench at NLR.

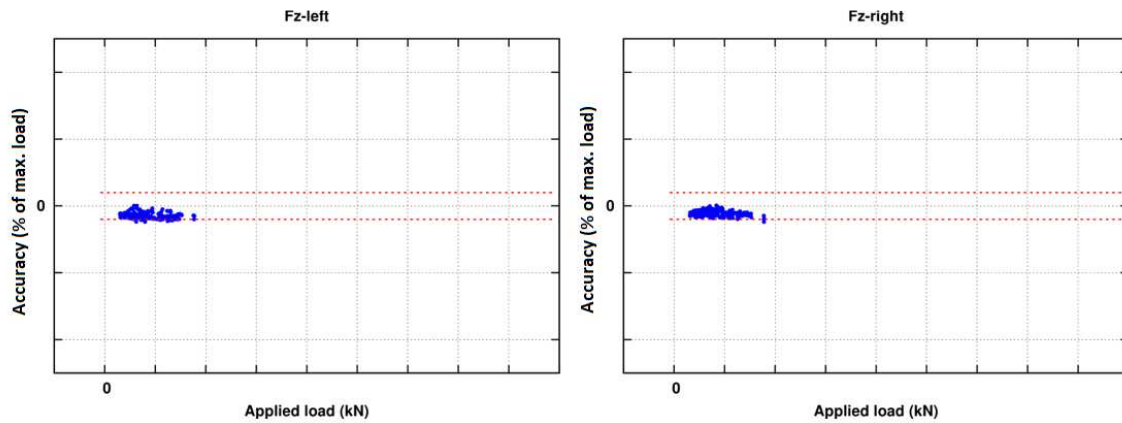


Figure 48 Example of load measurement accuracy.

6.2. Multiple load path damage detection with optical fibre Bragg grating sensors

F.P. Grooteman (NLR)

Many (aircraft) structures have multiple load paths where after a (partial) failure of a load path the remaining structure can carry the limit load without catastrophic failure or overly severe impact on the operational characteristics of the whole structure, until the structure is repaired, replaced or modified. A new damage indicator for structural health monitoring was developed that can detect a (partial) load path failure for a multiple load path structure, based on variable amplitude strain response measurements by fibre optic Bragg grating (FBG) sensors [36]. This fibre optic sensor is one of the most promising strain sensors for this purpose because it: is light weight, is tolerant for harsh environments (temperature, chemical components), has long term stability and durability, is completely passive and has no interference with other signals.

The damage indicator is defined as the ratio of the strain response summation of the strain time variation measured at all FBG sensors and a reference strain time variation measured at the same FBGs. Because the FBG strain response due to a load variation can be easily computed by means of finite element analysis, an optimal number, location and orientation of strain sensors can be easily derived for complex structures.

A test was performed on a box-shaped structure representative of a typical aircraft structure to validate the damage indicator, see Figure 49, demonstrating that the damage indicator is able to detect a damaged load path at an early stage of failure. From the simulation and test results it was concluded that the damage indicator is able to detect a damaged load path at an early stage of failure. It suffices to monitor each load path by only one strain sensor, although with more sensors damage may even be detected at an earlier stage. The damage size can be determined from the damage indicator value for a known damage scenario (as applied in the damage tolerance analysis), computed with finite element analysis, making it a level 3 SHM system. The presented damage indicator is not sensitive to temperature effects and therefore the SHM system does not require additional temperature sensors. Also, the damage indicator is not sensitive to the applied load time variation, making it robust. It can be computed on a flight-by-flight basis, drastically reducing the inspection interval. Moreover, it can distinguish a debonded sensor from a load path failure and a broken fibre or sensor can easily be detected by the sensor system, preventing falls calls.

The new damage indicator can be used in structural health monitoring applications of multiple load path structures like the wing structure consisting of multiple spars and a lower and upper skin that often can sustain a broken spar, the vertical stabilizer and wing attach fittings, a wing carry through bulkhead or engine mounts.



Figure 49 SHM test bench with double stiffened aluminium panel in climate chamber with the fibre optic interrogator (Gator, small red box) from PhotonFirst. The FBGs were mounted on the back side of the panel.

6.3. Structural Health Monitoring of Composite Structures by Fusing Sensor Data

Agnes Broer, Dimitrios Zarouchas, Rinze Benedictus, Nan Yue (TU Delft), Georgios Galanopoulos, Dimitris Milanoski, Theodoros Loutas (UPAT)

Composite structures are being increasingly used in the aerospace industry as primary aircraft structures. During their lifetime, the occurrence of damage is inevitable; it can occur due to material degradation caused by changing load and environmental conditions, as well as by unexpected events such as foreign object impacts. The (possibility of) occurrence of damage requires airlines to inspect and maintain their aircraft fleets following fixed-interval schedules or after incidents, potentially leading to unplanned or unnecessary maintenance. To mitigate the need for manual inspections, a solution can be to place permanent sensor networks on the aircraft structure that monitor the initiation and propagation of damage during service. The collected sensor data can then be used as input to diagnostic and prognostic models that assess the structural integrity and damage state of the composite structure. Yet so far, no permanent sensor networks can be found on the structures of commercial aircraft.

In our work, we develop a diagnostic methodology that is capable of monitoring damage on all four structural health monitoring (SHM) levels:

1. Does damage exist?
2. Where is damage located?
3. What type of damage is it?
4. How severe is the damage?

Moreover, we are investigating its extension towards prognostics:

- What is the remaining useful life of the structure?

In this manner, we aim to develop an integrated diagnostic-prognostic framework capable of assessing all five levels.

To develop such methodologies, experimental campaigns are being performed as part of the European H2020 project ReMAP (Real-Time Condition-based Maintenance for Adaptive Aircraft Maintenance Planning, <https://h2020-remap.eu/>). During these campaigns, we have tested single-stiffener composite skin-panels subjected to fatigue compression after impact tests. In future experimental campaigns, we will expand this towards multi-stiffener composite skin-panels, as well as a demonstration on a curved multi-stiffener panel. During each of these tests, we collect sensor data on the damage state of the composite structures using four SHM sensing techniques: 1) acoustic emission, 2) fiber Bragg gratings, 3) distributed strain sensing, and 4) Lamb waves. The test set-up at TU Delft is shown in Figure 50.

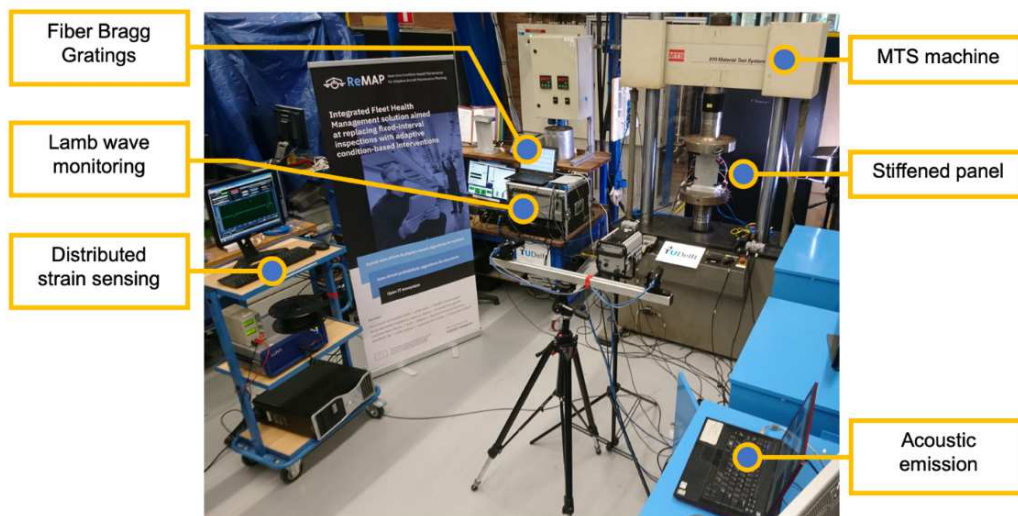


Figure 50 Test set-up at TU Delft.

For the development of the damage diagnostic and prognostic framework, we consider the inherent strength of each sensing technique and leverage this to our advantage. Here, it must be considered that not every technique is capable of monitoring all SHM levels and prognostics, nor that each technique is capable of assessing all damage observed in the composite structures. By combining them and fusing their data, we create a synergy that allows us to obtain a holistic damage assessment capable of answering all five questions.

So far, our work has focussed on the fusion of acoustic emission and distributed strain sensing data for damage diagnostics. Acoustic emission allows global monitoring of damage initiation and propagation, while the distributed strain sensing data allows for localized and precise tracking of stiffness

degradation and disbond growth. By fusing their data, we have shown that we can combine the strengths of each technique, resulting in both a global and local assessment of the damage growth, while simultaneously assessing all four SHM levels.

Future work will continue to elaborate on the development of an integrated diagnostic-prognostic structural health monitoring framework based on fusing sensor data from different sensing techniques. This will include, amongst others, extending the diagnostic framework to include the fusion with Lamb waves, as well as the further development of prognostic algorithms and their connection with diagnostics.

The first results of this work can be found in [37] and [38]. This work financially supported by the European Union's Horizon 2020 research and innovation program under grant agreement No. 769288.

7. Fleet Life Management

7.1. Individual tracking of RNLAF aircraft

Marcel Bos (NLR)

The Royal Netherlands Air Force (RNLAF) and NLR collaboratively keep track of the loads and usage of most aircraft types in the RNLAF inventory, viz. the F-16 Block 15, C-130H/H-30, NH90, AH-64D, ICH-47D and ICH-47F. This is done on an individual basis (individual aircraft tracking, IAT) and involves the installation of data acquisition and recording equipment, the development of modern data information systems and processing software, the development of fatigue and/or corrosion damage indices, the collection and processing of loads and usage data, the fusion of the collected usage data with the maintenance databases of the RNLAF to enable and enhance reliability analyse efforts, and the reporting of the processed data to the RNLAF. The results are used to:

- keep track of the consumed fatigue life;
- assess the severity of specific missions and mission types;
- evaluate and possibly optimize the usage of the fleets;
- optimize maintenance programs;
- assess/anticipate required structural modifications programs;
- provide the OEM with high-quality data in case of modification programs;
- rationalise decisions regarding tail number selection in the case of out-of-area deployment, fleet downsizing, decommissioning, etc.;
- develop load spectra for full-scale component testing;
- gain insight in the root causes of accidents and failures;
- enhance reliability analyses.

Many details of these programs were already supplied in previous National Reviews. A new activity is the development of an IAT-program for the AS-532U2 Cougar Mk.II transport helicopter fleet of the RNLAF, see Figure 51.



Figure 51 AS-532U2 Cougar Mk.II transport helicopter of the RNLAF.

8. Special Category

8.1. Impact of additive manufacturing on structural integrity methodologies

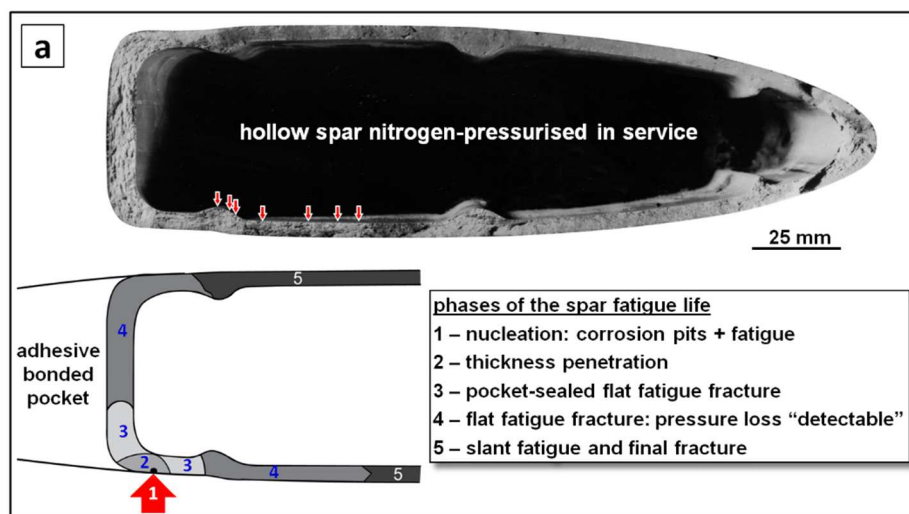
Ligeia Paletti, Emiel Amsterdam (NLR)

Approaches currently implemented in designing components produced by additive manufacturing (AM) create shapes that hardly fit in the existing, standardized methodologies used to assess structural integrity. The risk of assessing structural integrity in a conservative way is to hinder AM to realize its full potential and to make the implementation of AM non-competitive compared to traditional manufacturing. Within the aerospace environment, structural integrity is ensured by satisfying specific requirements. Methodologies developed to assess compliance with the requirements require several inputs, such as material properties, manufacturing methods, etc. A significant amount of work is in progress to produce input information specifically for AM, but limited investigations have been done on assessing the applicability of the methodologies themselves to AM-designed components. A paper has been written in which several aspects related to structural integrity assessments in aerospace are presented and their applicability to AM processes and components discussed [39]. Assumptions embedded in damage tolerance philosophies and existing damage tolerance requirements are evaluated, and alternatives are offered, with a particular focus on the importance of obtaining a good characterization of the (equivalent) initial flaw sizes in the product and the incorporation of load redistribution in the design and analysis phase.

8.2. Quantitative Fractography Applications for Fatigue Fracture Surfaces

Russell Wanhill (Emmeloord), Simon Barter (RMIT University, Melbourne)

This topic will be a chapter in a new edition of the ASM International Handbook Volume 12, Fractography, planned to be published in the Fall of 2021. The chapter provides examples of the application of QF to evaluate real life fatigue failures, and also a guideline chart, based on decades of fractographic experience, for detecting and measuring fatigue striations and progression markings. Most of the information in this article comes from experience with aerospace (aircraft) fatigue failures.



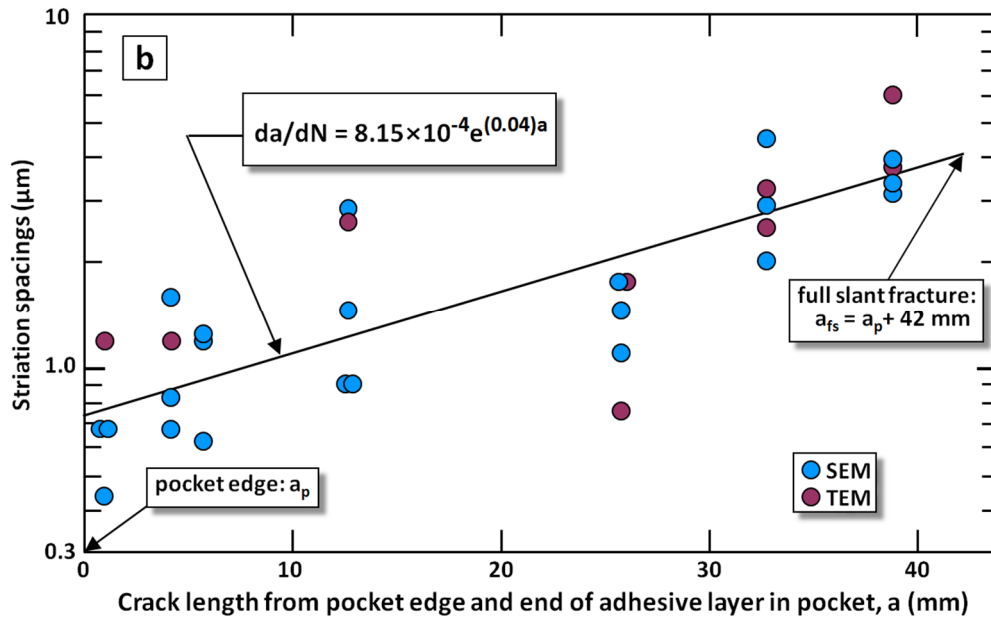


Figure 52 Fatigue failure of a Sikorsky S-61N helicopter pressurised rotor blade spar: (a) details of the fatigue fracture surface indicating the phases of the spar fatigue life and the locations (arrowed) of fractographs for striation spacing measurements; (b) SEM and TEM (surface replica) striation spacing measurements and the ‘best fit’ exponential FCG rate equation. After [40,41].

A Sikorsky S-61N helicopter crashed into the North Sea in May 1974, following fatigue failure of one of the five rotor blades. Figure Xa shows the inboard fracture surface of the failed blade, an AA6061-T6 aluminium alloy hollow spar normally pressurised with nitrogen, together with details indicating the phases of the spar fatigue life.

Figure 52 b) shows the results of fatigue striation measurements and the ‘best fit’ exponential equation representing the fatigue crack growth rates. The crack trajectory in Figure Xb represents the fatigue crack growth life available for in-flight crack detection owing to a pressure drop in the spar. The estimated number of cycles over this crack trajectory was used with Sikorsky design data to calculate the safe operating speed when an in-flight pressure loss is detected in any of the blades. This safe operating speed, 90 knots, was (very) conservative, based on giving a detectable fatigue crack growth life of 12 hours, about 4X the maximum duration of any flight by this type of helicopter.

8.3. Milestone case histories in aircraft structural integrity

R.J.H. Wanhill (ex-NLR) L. Molent and S. A Barter (ex-DST, Melbourne, Australia)

A chapter entitled ‘Milestone case histories in aircraft structural integrity’ has been prepared for publication in “Comprehensive Structural Integrity”, 2nd Edition, Volume I: Structural Integrity Assessment— Examples and Case Studies, Elsevier Ltd., Oxford, UK [42]. The chapter discusses six ‘milestone’ aircraft accident case histories: de Havilland Comet I crashes (1954); Boeing B-47(B,E) crashes (1958); General Dynamics F-111A crash (1969); Boeing 707-321C crash (1977); Boeing 737-297 accident/incident (1988); Aermacchi MB-326H crash (1990). Analyses and lessons learned from them have greatly improved the aerospace community’s capabilities in ensuring aircraft safety and

durability. Although these case histories have been especially influential, many others have contributed to developments in aircraft structural integrity. These developments are ongoing, and a summary is given, including the use of newer materials, notably carbon fibre reinforced plastic (CFRP) composites.

8.4. Short/small fatigue crack growth, thresholds and environmental effects

Russell Wanhill (Emmeloord), Stefanie E. Stanzl-Tschegg (Austria)

This paper [43] is the result of discussions about the review ‘When do small fatigue cracks propagate and when are they arrested?’ in *Corrosion Reviews*, 2019; 37(5): 397-418. These discussions arose from the two engineering paradigms characterizing fatigue research for (i) an aerospace research and technology remit for metallic airframes, and (ii) a materials science research programme supporting a methodology for steam turbine low pressure (LP) blade operations. This paper is in the spirit of August Thum (1881-1957), who collated, adapted and published much fatigue literature from different sources for the benefit of engineers and designers. The paper is of cross-discipline interest for investigators of metal fatigue with respect to design requirements, life predictions and assessments. In more detail, the paper considers the similarities and differences in the fatigue design methodologies for airframes and steam turbine LP blades, see Figure 53. This includes short/small fatigue cracks, fatigue crack growth thresholds, high-cycle fatigue (HCF) and very-high-cycle fatigue (VHCF), and the relevance of environmental effects (corrosion and corrosion fatigue).

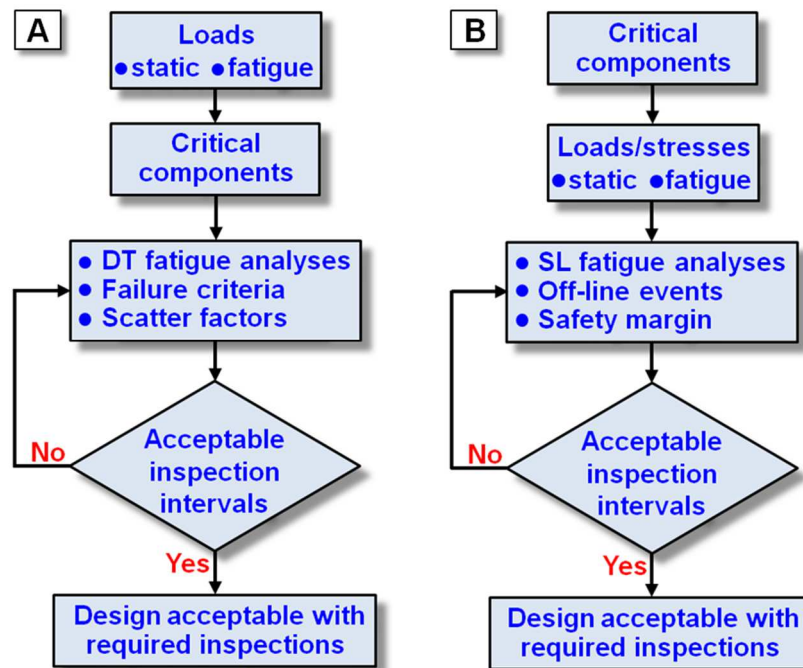


Figure 53 Schematics of the fatigue design methodologies for (A) Damage tolerance analyses for metallic airframes, and (B) Safe-Life analyses for 12% Cr steel steam turbine low pressure blades. The general similarities in approach are evident, while the first three stages of each flow chart are significantly different.

References

- [1] Van Kuijk, J. J. A., Alderliesten, R. C., Benedictus, R. (2021). Unraveling the myth of closure corrections: sharpening the definition of opening and closure stresses with an energy approach. *International Journal of Fatigue*, 143, 106016
- [2] Van Kuijk, J. J. A., Alderliesten, R. C., Benedictus, R. (2021). Measuring crack growth and related opening and closing stresses using continuous potential drop recording. *Engineering Fracture Mechanics*, (under review)
- [3] Van Kuijk, J. J. A. (2021). PhD dissertation, (in writing)
- [4] E. Amsterdam (2019) A novel fitting method to obtain fatigue crack growth rates without noise. 19th International ASTM/ESIS Symposium on Fatigue and Fracture Mechanics, Denver (USA), 2019. 1-5.
- [5] E. Amsterdam (2020) Effect of Crack Length and Reference Stress on Variable Amplitude Fatigue Crack Growth Rate. ICAF 2019 – Structural Integrity in the Age of Additive Manufacturing, Springer International Publishing. 539-550.
- [6] K.F. Walker, S. Stobart (2020) Summary and Findings from DST Group’s Military Transport Long Crack ASSIST Challenge. QPL-LR-00421.
<http://www.meetingdata.utcd Dayton.com/agenda/asip/2020/proceedings/presentations/P20086.pdf>
- [7] Smith, K. V. (2011). Application of the dissipated energy criterion to predict fatigue crack growth of Type 304 stainless steel following a tensile overload. *Engineering Fracture Mechanics*, 78(18), 3183-3195.
- [8] Klingbeil, N. W. (2003). A total dissipated energy theory of fatigue crack growth in ductile solids. *International Journal of Fatigue*, 25(2), 117-128.
- [9] R.J.H. Wanhill, S.E. Stanzi-Tschegg, Short/small fatigue crack growth, thresholds and environmental effects: a tale of two engineering paradigms, *Corros Rev* 2021.
<https://doi.org/10.1515/corrrev-2020-0096>
- [10] Kawai, M., and M. Koizumi. *Nonlinear constant fatigue life diagrams for carbon/epoxy laminates at room temperature*. *Composites Part A: Applied Science and Manufacturing*. 2007; 38:2342–2353. <https://doi.org/10.1016/j.compositesa.2007.01.016>
- [11] Kawai, M., and T. Murata. *A three-segment anisomorphic constant life diagram for the fatigue of symmetric angle-ply carbon/epoxy laminates at room temperature*. *Composites Part A: Applied Science and Manufacturing*. 2010; 41:1498–1510. <https://doi.org/10.1016/j.compositesa.2010.06.012>
- [12] Kawai, M., and N. Itoh. *A failure-mode based anisomorphic constant life diagram for a unidirectional carbon/epoxy laminate under off-axis fatigue loading at room temperature*. *Journal of Composite Materials*. 2014; 48:571–592. <https://doi.org/10.1177/0021998313476324>
- [13] Broer, A.A.R. and D. Zarouchas. *Adapted anisomorphic model for fatigue life prediction of CFRP laminates under constant amplitude loading*. *International Journal of Fatigue*. 2019; 126:270-283. <https://doi.org/10.1016/j.ijfatigue.2019.04.029>
- [14] Broer, A. A. R. *Fatigue life prediction of carbon fibre-reinforced epoxy laminates using a single S-N curve*. [Master of Science Thesis]. Delft, Netherlands: Delft University of Technology; 2018. <http://resolver.tudelft.nl/uuid:6c91fc86-f496-4ef1-bb1d-135f9497085b>
- [15] Lemaitre, J. (1984). How to use damage mechanics. *Nuclear Engineering and Design*, 80(2), 233-245. [https://doi.org/10.1016/0029-5493\(84\)90169-9](https://doi.org/10.1016/0029-5493(84)90169-9)
- [16] Reifsnider, K. (2012). “Fatigue of composite materials”. Elsevier, New York.
- [17] Van Ingen, J.W., Thermoplastic Orthogrid Fuselage Shell, *Sampe Journal* 52(5): 7-15, September (2016).

- [18] Van Dooren, K.S., Labans, E., Tijs, B.H.A.H., Waleson, J.E.A., and Bisagni, C., Analysis and testing of a thermoplastic composite stiffened panel under compression. Proceedings of the 22nd International Conference on Composite Materials (ICCM22), Melbourne, AU, August 11-16 (2019).
- [19] U.S. Department of Transportation, Federal Aviation Administration, Advisory Circular 20-107B, Change 1, Composite Aircraft Structure, August 24 (2010).
- [20] European Union Aviation Safety Agency, Acceptable Means of Compliance 20-29, Composite Aircraft Structure, July 26 (2010).
- [21] Renart, J., Budhe, S., Carreras, L., Mayugo, J. A., Costa, J. (2018). A new testing device to simultaneously measure the mode I fatigue delamination behavior of a batch of specimens. *International Journal of Fatigue*, 116, 275-283.
- [22] Reeder, J. R., Crews Jr, J. H. (1990). Mixed-mode bending method for delamination testing. *AiAA Journal*, 28(7), 1270-1276.
- [23] Berthelot J-M, Ei Mahi A, Le Corre J-F. Development of transverse cracking in cross-ply laminates during fatigue tests. *Compos Sci Technol* 2001;61:1711–21. doi:10.1016/S0266-3538(01)00068-9.
- [24] Maragoni L, Carraro PA, Peron M, Quaresimin M. Fatigue behaviour of glass / epoxy laminates in the presence of voids. In *J Fatigue* 2017;95:18–28. doi:10.1016/j.ijfatigue.2016.10.004.
- [25] Quaresimin M, Carraro PA, Maragoni L. Early stage damage in off-axis plies under fatigue loading. *Compos Sci Technol* 2016;128:147–54. doi:10.1016/j.compscitech.2016.03.015.
- [26] Alderliesten RC, Brunner AJ, Pascoe JA. Cyclic fatigue fracture of composites : What has testing revealed about the physics of the processes so far ? *Eng Fract Mech* 2018;203:186–96. doi:10.1016/j.engfracmech.2018.06.023.
- [27] Li X, Kupski J, Texeira De Freitas S, Benedictus R, Zarouchas D. Unfolding the early fatigue damage process for CFRP cross-ply laminates. *International Journal of Fatigue* 140, 105820 . <https://doi.org/10.1016/j.ijfatigue.2020.105820>
- [28] N. Eleftheroglou and T.H. Loutas. 2016. "Fatigue damage diagnostics and prognostics of composites utilizing structural health monitoring data and stochastic processes," *J. Struct. Health Monit.*, 15(4):473-488.
- [29] N. Eleftheroglou, D.S. Zarouchas, T.H. Loutas, R.C. Alderlisten and R. Benedictus. 2016. "Online remaining fatigue life prognosis for composite materials based on strain data and stochastic modeling," *J. Key Eng. Mat.*, 713:34-37.
- [30] T.H. Loutas, N. Eleftheroglou and D.S. Zarouchas. 2017. "A data-driven probabilistic framework towards the in-situ prognostics of fatigue life of composites based on acoustic emission data," *J. Compos. Struct.*, 161:522-5.
- [31] N. Eleftheroglou, D.S. Zarouchas, R. Benedictus 2020. An adaptive probabilistic data-driven methodology for prognosis of the fatigue of composite structures. *Composite Structures* 245, 112386.
- [32] N. Eleftheroglou, Adaptive prognostics for remaining useful life of composite structures, PhD Thesis, Delft University of Technology, 2020.
- [33] Grooteman FP (2020). Probabilistic Fail-Safe structural risk analyses, NLR Technical Publication TP-2020-416.
- [34] Nazeer N, Groves RM, Benedictus R. Simultaneous Position and Displacement Sensing Using Two Fibre Bragg Grating Sensors. *Proc. SPIE Smart Structures + Nondestructive Evaluation*. 2019; 10970: 109701Z–1 – 109701Z–8 <https://doi.org/10.1117/12.2513415>.
- [35] Nazeer N, Groves RM. Load Monitoring of a Cantilever Plate by a Novel Multi-modal Fibre Optic Sensing Configuration. Manuscript submitted for publication. 2020.

- [36] Grooteman FP (2020). Multiple load path damage detection with optical fiber Bragg grating sensors, NLR Technical Publication TP-2020-415.
- [37] Broer A.A.R., G. Galanopoulos, D. Zarouchas, T. Loutas, R. Benedictus (2021) Damage Diagnostics of a Composite Single-Stiffener Panel Under Fatigue Loading Utilizing SHM Data Fusion. In: Rizzo P., Milazzo A. (eds) European Workshop on Structural Health Monitoring. EWSHM 2020. Lecture Notes in Civil Engineering, vol 127. Springer, Cham. https://doi.org/10.1007/978-3-030-64594-6_60
- [38] Milanoski D., G. Galanopoulos, A. Broer, D. Zarouchas, T. Loutas (2021) A Strain-Based Health Indicator for the SHM of Skin-to-Stringer Disbond Growth of Composite Stiffened Panels in Fatigue. In: Rizzo P., Milazzo A. (eds) European Workshop on Structural Health Monitoring. EWSHM 2020. Lecture Notes in Civil Engineering, vol 127. Springer, Cham. https://doi.org/10.1007/978-3-030-64594-6_61
- [39] Paletti L, Amsterdam E (2019), Impact of additive manufacturing on structural integrity methodologies for aerospace components. First European Conference on Structural Integrity of Additively Manufactured Materials (ESIAM19), 9-11 September 2019, Trondheim, Norway.
- [40] R.J.H. Wanhill, S.A. Barter and L. Molent, Fatigue Crack Growth Failure and Lifting Analyses for Metallic Aircraft Structures and Components, SpringerBriefs in Applied Sciences and Technology, Springer Nature B.V., Dordrecht, The Netherlands, 2019
- [41] R.J.H. Wanhill, E.A.B de Graaf and W.J. van der Vet, Investigation into the cause of an S-61N helicopter accident. Part I: fractographic analysis and blade material tests, Report NLR TR 74103C, National Aerospace Laboratory NLR, Amsterdam, The Netherlands, July 1974.
- [42] R.J.H. Wanhill, L. Molent and S. A Barter, Milestone case histories in aircraft structural integrity. To be published in "Comprehensive Structural Integrity", 2nd Edition, Volume I: Structural Integrity Assessment— Examples and Case Studies, Elsevier Ltd., Oxford, UK.
- [43] Russell J. H. Wanhill, Stefanie E. Stanzl-Tschegg, Short/small fatigue crack growth, thresholds and environmental effects: a tale of two engineering paradigms, Corros Rev 2021; <https://doi.org/10.1515/correv-2020-0096>